DOCTORAL DISSERTATION

博士論文

Development of Uniform Eddy Current Probes using Multi Excitation Coils

マルチ励磁コイルを用いた一様渦電流プローブの開発

16 TF 904

AGENG SADNOWO REPELIANTO

（アグンサッノウォルプリヤント）

Supervisor

Assoc. Prof. NAOYA KASAI

Graduate School of Environment and Information Sciences
Yokohama National University

March 2020

DOCTORAL DISSERTATION

Development of Uniform Eddy Current Probes using Multi Excitation Coils

Submitted by
AGENG SADNOWO REPELIANTO

Supervised by
Assoc. Prof. NAOYA KASAI

Graduate School of Environment and Information Sciences
Yokohama National University

March 2020

DOCTORAL DISSERTATION

Development of Uniform Eddy Current Probes using Multi Excitation Coils

Dissertation approved:

1. Assoc. Prof. Naoya KASAI
   Academic Supervisor

2. Prof. Hideo OTANI
   Committee Member

3. Prof. Atsumi MIYAKE
   Committee Member

4. Prof. Shinji OKAZAKI
   Committee Member

5. Prof. Tadahiro SHIBUTANI
   Committee Member

Abstract

Many fatal accidents such as; the explosion of gas pipes collapse of structures of the factory, tearing of the fuselage caused by a crack that was initially small crack. As a result of the tensile or compressive forces acting on the structure, over time, the appearance of cracks will grow and cause the fracture toughness to decrease quickly and indefinitely. Predicting the exact time of the appearance of a flaw is impossible. However, the work periodically checks for detecting the appearance of a flaw or predicts its behaviour at a location and dimensions are a necessity. This activity is an inspection to guarantee the quality of physical products or structural components in the process activities in its standard requirements. Non-destructive inspection or classified as non-destructive testing (NDT) has the general advantage of being low-cost, saving evaluation time and especially not changing the shape or characteristics of the test object along in evaluation.

One of the NDT methods is the electromagnetic method or the eddy current method. The principle of this method is the process of inducing a magnetic field into the test object. The object's response to the magnetic field translated to predict the characteristics of the test pieces. Furthermore, the phenomenon of the measurement targeted is the presence and dimensions of the flaws. Initially, eddy current probes use a single coil as a sensor [1], the working principle of the probe measures the change in impedance that occurs when testing. The detection signal from this probe is powerful but cannot be used to predict the depth of the flaw that produces much noise due to the lift-off effect. Following that, the EC probe model developed with a separate receive-transmission eddy current probe model consisting of two separate coils as exciter and as a detector. This separation effective to reduce the effect of lift-off and can be potential to predict the depth of the flaws. However, the signal is weak and requires a signal amplifier circuit. Besides, confidence for the measurement results of flaw depth is still low.

The next focus is to obtain a reliable flaw depth measurement. The design of the Hoshi probe as the first Uniform eddy current (UEC) probe developed. This probe consists of an excitation coil with tangential orientation, and a detector coil positioned pancake to obtain unique characteristics of self-differential and self-nulling.

These characteristics will only produce a detection signal when a flaw detected. Meanwhile, the signal amplitude represents information of the depth of flaw. The concept of tangential excitation coil has given the idea to several other UEC probe models. Based on the circulating of eddy current generated, all models are grouped into two types of

probes. First is one-directional UEC probes that have UEC circulations only one direction alternating. Second is the rotating UEC probe that has the direction the circulation is one-way and rotating.

The structure of one direction probe is more straightforward but in practice, its application requires twice scanning process in the x and y direction, to satisfy the test standards. Meanwhile, the second type of probe structure has a bit complex, but the scanning is faster, which do only one direction, the x-direction or the y-direction, so it saves time. However, all those probes ware still unsatisfied because their detection signals are small and require an amplifier circuit. This small signal detection was a limitation to detect for smaller flaws dimensions.

In this study, a new UEC probe design that has multiple excitation coils and a detector coil which are all pancake oriented have self-differential, and self-nulling characteristics presented. The model has simulated, and the experimental verifications have done. The aim of the developed of the new UEC probe is to improve detection signals and immune with the effect of lift-off. The magnetic field of the double excitation coils succeeds to generate a large uniform eddy current, which makes the opponent's magnetic field also increase. As a result, the induction to the detector coil also increases. The new UEC probe called the Butterfly probe made for two types; One-directional Butterfly probe and Rotating Butterfly probe.

The simulation resulted show the success where the induction of the Butterfly probe increased significantly approximately 1.8 times compared to conventional UEC probes with the tangential excitation coil. The simulation also succeeded in showing eddy current circulation patterns from the One-directional Butterfly probe and the Rotating Butterfly probe following its hypothesis.

Experimental verification has shown satisfying results where the detection signal containing clear two peaks. The distance between of peaks represents the flaw length and the signal amplitude proportional to flaw depth. The low amplitude, which is close to zero between the two peaks indicates that the probe has self-differential and self-nulling properties. Meanwhile, the Rotating Butterfly Probe has succeeded to detect flaws with various orientation.

Acknowledgement

Something extraordinary, I obtain during my studies. It all starts at the opportunity and processes in the best guidance and support provided by my supervisor. For all of that, I would like to thank assoc Prof. Naoya Kasai.

I also to thank Prof. Tadahiro SHIBUTANI, who initiated the weekly meeting of Doctor students to present research progress, and to all members of the meeting, who provided technical advice for the best achievement to my studies.

I am grateful to all my doctoral dissertation committees: Prof. Hideo OTANI, Prof. Atsumi MIYAKE, and Prof. Shinji OKAZAKI for all the comments that sharpened the writing of my doctoral dissertation and stimulated me to develop future research ideas.

Especially for the Uniform Eddy Currents research team, I am thankful to Dr. Kouichi SEKINO, Matsunaga MASAKI and Le Quang Trung who technically have helped to make simulations, procure test material and collect experimental data. This assistance was helpful and make efficient my research work time.

To the BUDI (Excellence for Indonesian Lecturers)-LPDP (Educational Funds Agency) scholarship grantor, I would like to thank for the opportunity for funding my doctoral studies in Japan. This opportunity is something more special throughout my level of study. Thanks also to the University of Lampung for permission and valuable support to I took this opportunity.

Finally, especially to my family: My wife Anna Andiani, my children, that accompany as long stay in Japan: Aufa Ahsannur Dzarofiq and Ainhayya Najmi Rumaisya and my daughter eldest that should be separated in Indonesia Ainur Yasmin Shofurra. All of you are my energy that never dies.

Statement of Originality

I hereby certify that this dissertation and the research supporting this study are the product of my own work. The work performed by other research groups and individuals is fully acknowledged as references in this dissertation.

Ageng Sadnowo Repelianto

January 14, 2020

TABEL OF CONTENT

Chapter 5

LIST OF TABLES

LIST OF FIGURES

NOMENCLATURE

A : Magnetic vector potential of coil in the space (Tm)
B : Magnetic flux of coil (T)
H : Magnetic field of coil (A/m)
J : Eddy current in test piece (A)
V : Potential difference on test piece (V)
E : Electric fields that arise due to changes in magnetic fields (V/m)
μ : Permeability of test piece (H/m)
σ : Conductivity of conductor (S/m)
Φ : Magnetic flux of coil (Wb/m^2)
ε : Electromotive force on detector coil (V)
S : Surface area of interaction (m^2)
l : Length of wire of a coil (m)
Z_o : The impedance of an excitation coil on the air (Ω)
Z_c : The impedance of an excitation coil on the test piece (Ω)
v_o : Voltage input of the excitation coil on the air (V)
i_o : Currents in the excitation coil on the air (A)
R_o : The resistance of the excitation coil on the air (Ω)
R_c : The resistance of the excitation coil on the test piece (Ω)
R_e : The resistance of the test piece in the equivalent circuit (Ω)
jX_o : The reactance of the excitation coil on the air (Ω)
jX_c : The reactance of the excitation coil on the test piece (Ω)
jX_m : The reactance of the test piece in the equivalent circuit (Ω)
L_o : The inductance of the excitation coil on the air (H)
L_1 : The inductance of the excitation coil on the air (H)
f : Frequency of excitation signal (Hz)
ω : Angular frequency (Hz)
I : Currents in the primary equivalent circuit of the excitation coil (A)
I_e : Currents in the closed equivalent circuit of the test piece (A)
M : Mutual induction (H)
k : The ratio between both coils L_o and L_1
φ : Phase

Chapter 1
1. Introduction

1.1. Background

Flaws in structural components are conditions caused by tensile forces or compressive forces working on the structure. The appearance of a flaw is a sign of hazard. Over time, the flaw will grow and reduce the strength of the fracture so that it can cause serious damage.

Flaws are defined as imperfections or discontinuities that can be detected by non-destructive testing and cannot always be rejected according to the American Society for Testing and Materials (ASTM) E1316-17a standards.

An impossible to predict the exact timing of the emergence of a flaw. But the work of predicting the behavior of flaw in a location, and its dimensions are a necessity. To guarantee the quality of a physical product or components of the structure in the process activities in its standard requirements, inspection activities are carried out.

Inspection is a process of checking visually or involves sensing sensors. Inspection activities include measurements and tests that follow the specific characteristics of the standard requirements that guarantee quality control of a product or process activity. Usually, the nature of these inspections is non-destructive or classified as non-destructive testing (NDT). NDT has the general advantage of being low-cost,

saving evaluation time and notably no changing the shape or characteristics of the test object in its evaluation. There are eight popular NDT methods used in their application. Each method has a typical working principle to fulfil the demands of precise measurement specifications in evaluation services.

One of the nondestructive testing methods is the electromagnetic testing method. This method performs the process of inducing a magnetic field into the test object. The object's response to the magnetic field can describe definite characteristics of the object. The phenomenon of objects that are become the target of measurement is the existence and dimensions of the flaw.

1.2. Eddy current testing in NDT

Existing electromagnetic methods are used such as eddy current testing (ECT), remote field testing, magnetic flux leakage testing, magnetic particle inspection and alternating current field measurement.

The popular electromagnetic method developed in NDT is eddy current testing. This testing is an old testing method. However, since the last two decades, it has been developing because of its potential ability are quick, versatile, sensitive, does not require preparing of surface, and is easily adapted to the automation of test devices.

The growing demands of the ability of the testing probes like as increasingly high for standard criteria, and the ability of special functions for scanning of increasingly diverse material characteristics, these demands make the researchers continue to conduct studies to develop new probe models.

In the beginning, the eddy current probe was a single-coil type, the probe consisted only of an excitation coil which also functioned as a detection coil. The working

principle of the probe measures the change in impedance that occurs in the probe when a phenomenon changes the test object characteristic [1]. This Probe model is simple, easy and produces a detection signal that is strong enough for the evaluation criteria to detect the location of the flaw and predict the length of the flaw. However, this type of probe has the disadvantage of being unable to predict the depth of a flaw. The effect of the lift-off of the coil on the test object significantly affects the impedance. Thus, the measurement results are fake.

The transmit-received probe model was developed. The probe consists of two coils, the excitation coil and the detection coil. The coil function separation is to reduce the effect of the lift-off on the excitation coil when measuring. This method was successful in reducing the effect of lift-off. However, the detection signal becomes weak. It takes more excitation power to increase the detection signal. Besides, the confidence for the flaw depth measurement results is still low, because although the effect of the lift-off has reduced, it still has a significant effect on the ratio of signal to noise, where the detection signal is low [2].

In 1996, Hoshikawa and Koyama presented a Uniform eddy current (UEC) probe. The probe consists of two separate coils, the excitation coil and the detection coil. Excitation coil with tangential orientation and detection coil with pancake orientation positioned in the center of the excitation coil [3]. This position is the essence of this model. With this concept, the eddy current that appears below the excitation coil has a relatively uniform amplitude intensity. This condition causes the detection signal arises by the detection coil to have the characteristic of keeping electromotive force (EMFs) generated on the coil parts or called self-differential characteristics. Because of these characteristics, in a balanced EMFs condition on the parts of the detection coil, the resulting detection signal is zero, which is said to be a self-nulling characteristic. This concept can produce

reliable flaw depth measurement signals. However, the tangential orientation of the excitation coil causes the detection signal to become weak. So, it requires a signal amplifier circuit.

At present, demands for NDT instruments such as eddy current probes are moving towards portable, low-power devices, long battery operation times, high sensitivity, and it can detect flaws that are getting smaller and buried. This challenge is the basis for the authors to research developing a new UEC probe with a double excitation coil trend and has self-differential and self-nulling properties.

1.3. Motivation and Objectives

Motivation

The primary motivation of this research is to answer the question, can a new UEC probe be designed with two advantages, have high sensitivity and trust to predict the depth of a flaw? Both of advantages are a combination of advantages possessed by conventional EC probes that have strong induction capabilities to produce high sensitivity to detect a flaw, with the advantages possessed by the UEC probe which has the confidence to measure the depth of a flaw.

Objectives

The main objective of this research is to develop a UEC probe which has a strong induction, thereby increasing the sensitivity of the UEC probe and the probe has differential and self-nulling characteristics. The research activity has five specific objectives as follows;

- To identify the shape and orientation of the UEC probe structure to improve detection capabilities;

- To design and observe the one-directional UEC probe with a pair of the rectangular excitation coil and a circular detection coil in which all coils are pancake oriented;
- To design and observe a rotating UEC probe with two pairs of the rectangular excitation coils and a circular detection coil with all of the coils are pancake oriented;
- To validate the UEC probe developed has self-differential and self-nulling properties and its sensitivity have increment.

1.4. The Outline of Dissertation

This dissertation divided into 5 chapters. Chapter 1 briefly presents the background, motivation, goals, work contributions and achievements of the research. This research explores the development of a UEC probe to detect flaws on aluminium material to possess a more sensitive detection capability. The proposed probe model is a separate transmit-received probe type using multiple coils. The working principle of the probe is to generate eddy current in one direction. Besides that, it also proposed the second model that uses principle a rotating eddy current.

Chapter 2 briefly presents a literature review related to theoretical of EC, the principle of testing eddy currents for detecting flaws, factors that influence the sensitivity. Study of UEC probe configuration, UEC characteristics, self-differential and self-nulling detector characteristics, and two types of UEC distributions; one direction UEC and rotating UEC.

Chapter 3 presents a new one-way directional UEC probe design with a pair of pancake-oriented excitation windings and has self-differential and self-nulling characteristics. Design simulations and experiments carried out to scan flaws in aluminum plates show a significant increase in the sensitivity.

Chapter 4 presents a new design of a rotating UEC probe with two pairs of excitation coils pancake-oriented and has self-differential and self-nulling characteristics. The simulation show the rotation of the eddy current distribution, and experiments carried out shown the ability of the probe to detect flaws with two orientations, perpendicular and parallel against the length of flaws.

Chapter 5 is the conclusion. It presents summarizing the significant results obtained from this research work. Recommendations for the development of two new UEC designs with multi-oriented pancakes presented.

Chapter 2
2. Study on the Configuration of Uniform Eddy Current (UEC) Probes

2.1. Introduction

Eddy current (EC) technique is one fundamental electromagnetic nondestructive evaluation technique [4-6]. This technique is common widely used in industries like a power plant, aerospace, petrochemical and other industries. One popular using of it is to evaluate the size of flaws on the surface or sub-surface flaws in components made of metallic materials [8-11]. Besides, it is also used traditionally for assessing the adequacy of heat treatment of alloys, as eddy currents are sensitive to changes in microstructure and stresses, electrical conductivity and magnetic permeability of the material [1]. To date, researchers in both academe and industry continue to investigate and develop new eddy current probes to achieve high signal-to-noise (S/N) ratios to be able to predict the size of the increasingly smaller flaws. [7-8].

2.2. Eddy Current Technique

Eddy current testing (ECT) is a useful way to detect fatigue cracks in the conductive

material. Many advantages, such as high sensitivity, fast scanning, non-contact inspection, and flexibility, contribute to their extensive utilization [12]. It was also able to test surface flaws that have layers without having to remove layers [13, 14]. However, demands in the future demand to further enhance the diagnostic capability of detection of eddy current probes to become more sensitive and more complex testing reference standards, this condition requires the development of techniques and the development of application instruments also. For this reason, development in the field of surface flaw testing expected to contribute to the user community.

2.2.1. Eddy Current generating principle

In principle, the eddy current technique is the pattern of the relationship between the magnetic field exciter and conductive material. The principle of generating a detection signal from the detection coil follows Maxwell's law, as illustrated in Figure 2.1. When a coil in the airspace and current $i(t)$ flows, then the potential magnetic vector A appears in the space (x, y, z).

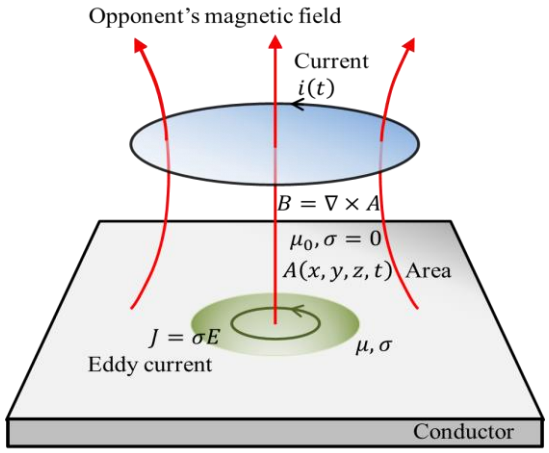

Figure 2.1 Coil and conductor.

The relationship between the current density *J* and the magnetic vector potential *A* is as given in equation (2.1).

$$A = \frac{\mu}{4\pi}\int_V \frac{J}{r}dV \tag{2.1}$$

The relationship between magnetic vector potential *A* and magnetic flux density *B* is as shown in equation (2.2).

$$B = \nabla \times A \tag{2.2}$$

Therefore, when a conductor arranged under the coil, an electric field *E* is generated according to equation (2.3). Next, the eddy current *J* is generated by this electric field (2.24), where, σ is the conductivity of the conductor.

$$\nabla \times E = -\frac{\partial B}{\partial t} \tag{2.3}$$

$$J = \sigma E \tag{2.4}$$

The magnetic field is generated by the current *i*(*t*) on the coil, and the magnetic field that arises because the eddy current determines the overall magnetic field. Then, this magnetic field produces electromotive force in the test coil, as shown in Eq. (2.5). Therefore, this concept is the concept of generating electromotive force ε in the test coil.

$$\varepsilon = -\frac{d\Phi_B}{dt}$$

$$\varepsilon = -\frac{d}{dt}\int B \cdot dS \tag{2.5}$$

Another idea is that the electromotive force ε in a coil caused by the electric field generated along the windings of the coil, as shown in Eq. (2.6).

$$\varepsilon = \oint_C E.dl$$

$$\varepsilon = \oint_C \left(-\frac{\partial A}{\partial t}\right) dl \tag{2.6}$$

When the test coil arranged positioned close to the conductor, as shown in Figure 2.2, the electric field in the conductor corresponds to the eddy current distribution, in which the component of the electric field in the direction of the eddy current contributes to the electromotive force.

The shape of the excitation coil determines the distribution of eddy currents. Consequently, there is a relationship between the electromotive force that appears with the shape of the coil winding. Therefore, the design of the test coil shape will determine its characteristics [15, 16].

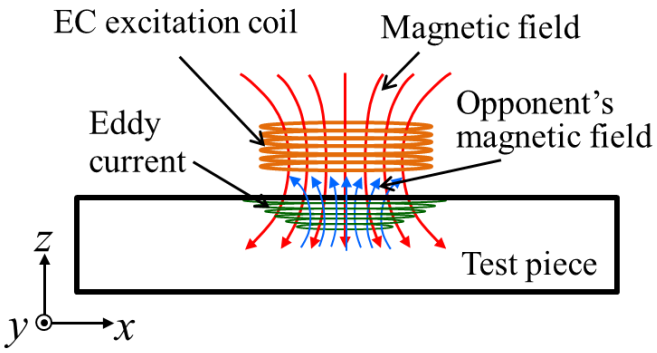

Figure 2.2 Principle of eddy current technique.

Furthermore, its interaction with physical phenomena in conductor can cause eddy

current distribution patterns to change. This changing affects the opponent's magnetic field pattern, which will eventually be captured and interpreted as a phenomenon of the conductor.

The principle of simplicity, the magnetic exciter field is a coil that equivalent to an impedance Z_o. It is a complex number parameter, as shown in equation (2.7). This impedance is the ratio of the excitation voltage v_o to the frequency f and the current i_o flowing in the coil. In phasor diagram, it has magnitude | Z | and phase φ, as shown in equation (2.8).

$$Z_o = {}^{v_o}/_{i_o} = R_o + jX_o = R_o + j2\pi f L_o \tag{2.7}$$

$$Z_o = \sqrt{R_o^2 + X_o^2} = |Z|_\varphi \tag{2.8}$$

When the excitation coil approaches the conductive test material, the interaction between the two causes the induction occurs and changes the coil impedance of Z_o to Z_c, as shown in equation (2.9):

$$Z_c = R_c + jX_c = R_c + j2\pi f L_c \tag{2.9}$$

where R_c, X_c, and L_c represents the new of real number, imaginary and inductance coils respectively. The difference between Z_o and Z_c is then the basis for the interpretation of the physical phenomena of the test piece [17].

2.2.2. Eddy Current Equivalent Circuit Model

To understand, the interaction between the excitation coil and the test pieces, this situation is modelled with the equivalent transformer circuit, as shown in Figure 2.3. The primary circuit consists of R_o and L_o components representing the excitation coil while the closed circuit with components L_o and $R_e + jX_m$ represent the test pieces. A resistor R_e representing the resistivity of the test piece and an imaginary part jX_m representing

the mutual induction of a closed circuit. Mutual coefficient k is a representation of the effect of the distance between the coil and the test object [17].

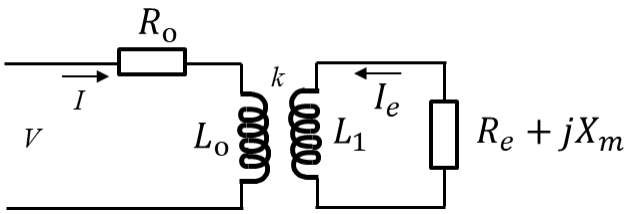

Figure 2.3 Equivalent circuit of interaction coil and test piece based on a transformer.

Following Kirchoff's law, the equivalent circuit is expressed by equations (2.10) and (2.11):

$$R_o I + j\omega L_o I - j\omega M_2 I_e = v \tag{2.10}$$

$$R_e I_e + jX_m I_e + j\omega L_1 I_e - j\omega M_1 I = 0 \tag{2.11}$$

where ω is $2\pi f$. M_1 and M_2 are the mutual induction of both inductors L_0 and L_1. $M_1 = kL_0$ and $M_2 = kL_1$. Furthermore, Association of equation (2.10) results (2.12).

$$I_e = \frac{j\omega M_1 I}{R_e + jX_m + j\omega L_1} \tag{2.12}$$

Then we substitute equation (2.12) to (2.10), and we were obtained Z_c.

$$R_0 I + j\omega L_0 I - j\omega M_2 \left(\frac{j\omega M_1 I}{R_e + jX_m + j\omega L_1}\right) = v \tag{2.13}$$

$$\left(R_0 I + j\omega L_0 I - \frac{j^2\omega^2 M_1 M_2}{R_e + jX_m + j\omega L_1}\right) I = v \tag{2.14}$$

$$Z_c = {}^{v}/_{I} = R_0 + j\omega L_0 + \frac{\omega^2 M_1 M_2}{R_e + jX_m + j\omega L_1} \tag{2.15}$$

$$Z_c = R_0 + jL_0\omega + \frac{k^2 L_0 L_1 \omega^2}{R_e + j\omega L_1 + jX_m} \tag{2.16}$$

When the coil is free without being close to the test piece, the mutual coefficient k is zero, so Z_{o} is the same as equation 2.7. Then when the coil is positioned above the test piece surface, the coil impedance becomes Z_{c}, as shown in equation (2.16).

Furthermore, from equation (2.16) the inductance and resistivity characteristics of the primary circuit reduced to obtain values of the inductance and the resistivity of the primary coil.

$$Z_{\mathrm{c}} = R_0 + jL_0\omega + \left(\frac{k^2 L_0 L_1 \omega^2}{R_e + j(\omega L_1 + X_m)}\right)\left(\frac{R_e - j(\omega L_1 + X_m)}{R_e - j(\omega L_1 + X_m)}\right) \tag{2.17}$$

$$Z_{\mathrm{c}} = R_0 + jL_0\omega + \left(\frac{k^2 L_0 L_1 \omega^2 R_e - jk^2 L_0 L_1 \omega^2 (\omega L_1 + X_m)}{R_e^2 + (\omega L_1 + X_m)}\right) \tag{2.18}$$

$$Z_{\mathrm{c}} = R_0 + jL_0\omega + \left(\frac{k^2 L_0 L_1 \omega^2 R_e}{R_e^2 + (\omega L_1 + X_m)}\right) - \left(\frac{jk^2 L_0 L_1 \omega^2 (\omega L_1 + X_m)}{R_e^2 + (\omega L_1 + X_m)}\right) \tag{2.19}$$

$$Z_{\mathrm{c}} = \underbrace{R_0 + \left(\frac{k^2 L_0 L_1 \omega^2 R_e}{R_e^2 + (\omega L_1 + X_m)}\right)}_{R_{\mathrm{c}}} + \underbrace{jL_0\omega - \left(\frac{jk^2 L_0 L_1 \omega^2 (\omega L_1 + X_m)}{R_e^2 + (\omega L_1 + X_m)}\right)}_{X_{\mathrm{c}}} \tag{2.20}$$

Thus for R_{c} and R_{c} are:

$$R_{\mathrm{c}} = R_0 + \left(\frac{k^2 L_0 L_1 \omega^2 R_e}{R_e^2 + (\omega L_1 + X_m)}\right) \tag{2.21}$$

$$X_{\mathrm{c}} = jL_0\omega - \left(\frac{jk^2 L_0 L_1 \omega^2 (\omega L_1 + X_m)}{R_e^2 + (\omega L_1 + X_m)}\right) \tag{2.22}$$

Both of equations (2.21) and (2.22) show that the coil characteristics change due to the appearance of eddy currents. Where the value of the coil resistivity increases marked by the operation sign '+' in the second term of (2.21). While the value of the coil inductance decreased, it showed by operation '–' in the second term of (2.22).

In addition, *k* as the coefficient of representation of the distance between the coil

and the test piece becomes something that affects the measurement results, where it called the effect of lift-off [17].

2.3. UEC Technique

In the case of tests carried out for test plate pieces with coated surfaces or uneven surfaces such as in weld areas and detection locations at the edges, conventional ECTs confront challenges where the detection signal produces much noise. This noise generally effected by lift-off. For this reason, it is essential to develop eddy current probes that are resistant to noise interference [10, 18].

Furthermore, future eddy current probe modification demanded higher detection capabilities with unique features such as self-nulling, self-nulling and noise-free of lift-off. The proposed design uses the UEC concept in which eddy currents have a straight-line pattern in part of its distribution. This pattern differs from the circular eddy current pattern of the conventional EC probes. To obtain this pattern, the geometry of the exciter probe coil must in tangential positioned, while the geometry of the detector coil can be in tangential or pancake position. The UEC probe design provides small lift-off noise and a steady phase signal. This information is a guarantee of confidence for predicting quantitative measurements of flaw depth [10, 12, 14, 17, 19, 20].

2.4. Characteristics of UEC

Conceptually, the UEC has an eddy current flowing in a straight-line pattern which is generated by the tangential rectangular excitation coil. Figure 2.4(a) shows the sectional view, indicating the flow of the UEC and magnetic flux of the tangential excitation coil. A tangential rectangular excitation coil with alternating current supply generates a magnetic field, and the eddy current is induced on the surface of the test piece.

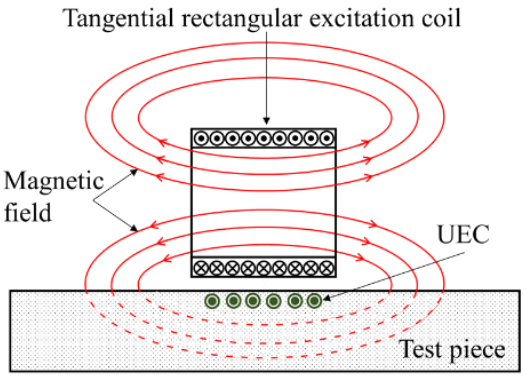

(a)

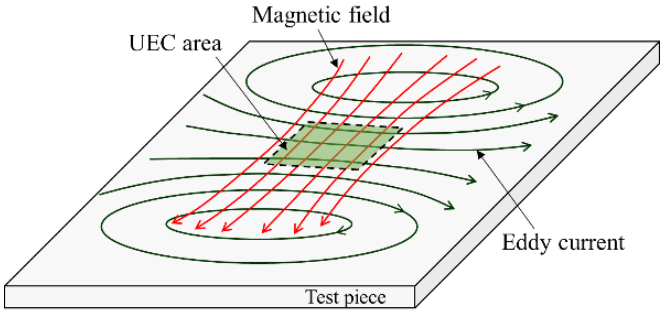

(b)

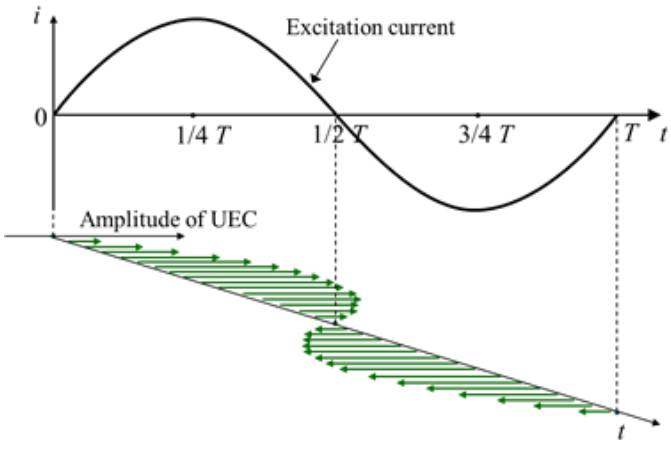

T: Period

(c)

Figure 2.4 Principle of generation of the UEC. **(a)** Sectional view indicating the flow of the UEC and magnetic flux of the tangential excitation coil. **(b)** UEC area on the surface of the test piece. **(c)** Relationship between the excitation current and the amplitude of the uniform eddy current on the UEC area.

The UEC flows on the surface of the test piece, parallel to the winding direction of the excitation coil. The uniform eddy current occurs in straight lines perpendicular to the magnetic fields, which are in a specific area, green box dot line of Figure 2.4(b). As the amplitude of the excitation current changes, the induced eddy currents have a uniform amplitude with one-direction, whose polarity changes every half cycle of the period as shown in Figure 2.4(c).

Based on the eddy current flow pattern in the test piece, the probe design is divided into two types—one-direction UEC and rotating UEC. The one-direction UEC pattern is produced by a tangential rectangular excitation coil or a magnetizer [18, 20]. Rotating eddy currents can be generated by a combination of two excitation coils or two magnetizers arranged crossed orthogonal to one another. Two excitation currents with a phase difference of 90° are used. Further explanation of both types is in the following section.

2.5. Self-Differential and Self-Nulling Characteristics

A probe using UEC phenomena generally has a unique property the output due to the change of the local conditions of the test piece, such as lift-off, is cancelled. This is called a self-differential characteristic. The property which makes a probe in balance so that the output of a detector coil is zero in normal conditions is known as a self-nulling characteristic.

When the UEC flows under the detector coil, in the part of the coil winding like an arc and parallel to the direction of the eddy current flow arises the electromotive force (EMF) ε on both parts of the coil, ε_1 and ε_2. Ideally, the amplitudes of them are the same, but differ in polarity. Hence, they cancel each other out. In balance conditions the EMFs is zero, due to the self-nulling property [20]. To understand this mechanism is

illustrated in Figure 2.5, and next represented in the following equation.

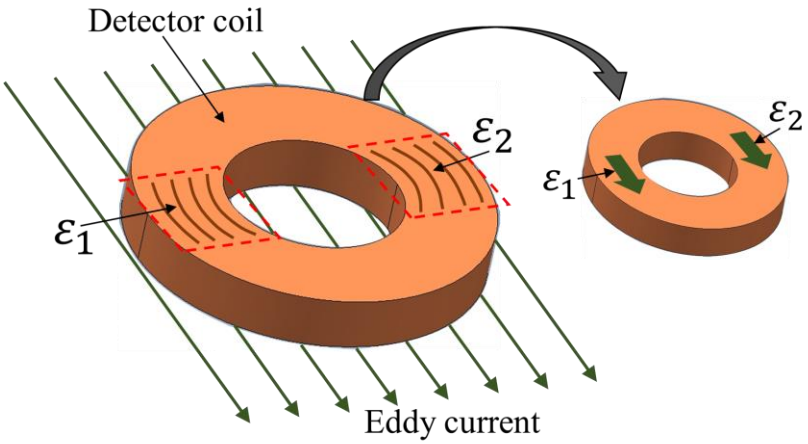

Figure 2.5 Illustration of self-differential and self-nulling properties.

We can assume that the electromotive force coil is the sum of the integration paths of ab, bc, cd and da as in equation (2.20).

$$\varepsilon = \oint_C E.dl$$

$$\varepsilon = \int_a^b E.dl + \int_b^c E.dl + \int_c^d E.dl + \int_d^a E.dl \tag{2.20}$$

In Figure 2.6, the part of the integration path of the coil that tends to be parallel to the direction of the eddy current is the *bc* and *da* integration paths. Therefore, these paths have the potential to be induced by the generated magnetic field. On the other hand, the *ab* and *cd* integration paths tend to be perpendicular to the direction of eddy currents, so these integration paths cannot be induced. Next, the equation becomes (2.21).

$$\varepsilon = \int_b^c E.dl + \int_d^a E.dl \tag{2.21}$$

$$\varepsilon = l(E_{bc} - E_{da}) \tag{2.22}$$

Assume,

$$\varepsilon_1 = lE_{bc}\ ;\ \varepsilon_2 = lE_{da} \tag{2.23}$$

then,

$$\varepsilon = \varepsilon_1 - \varepsilon_2 \tag{2.24}$$

where ε is the EMFs of the detector coil, ε_1 is the EMFs on the left integration path of the coil, and ε_2 is the EMFs on the right integration path of the coil.

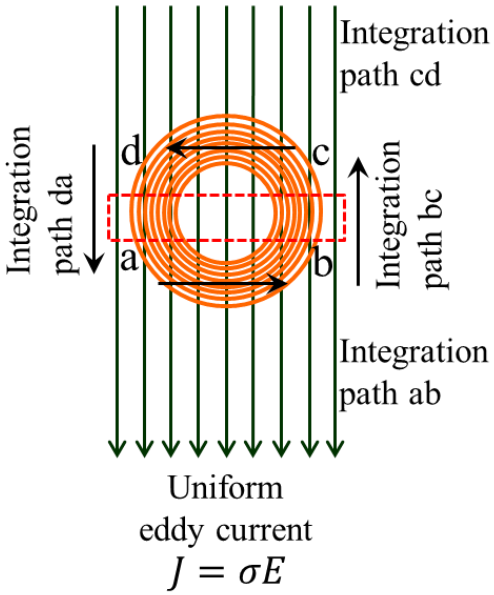

Figure 2.6 Generating of the electromotive force on detector coil over UEC.

Furthermore, when there is lift-off variation, the eddy current will be changing, affecting the EMFs on both sides through opposite magnetic fields [18, 21]. Even though both the EMFs values change, the amplitude of both remains the same. Therefore, the output of the coil remains at zero due to them cancelling each other. The ability to eliminate the influence of lift-off is the critical advantage of the UEC probe technique.

2.6. Apparatus of the UEC System

There are two types of UEC probe operational support systems, as previously mentioned: apparatus for a one-direction UEC, and apparatus for a rotating UEC. For the one-direction type, the system consists of a function generator, a power amplifier, a UEC probe, a signal amplifier with filter, and a phase lock-in amplifier, as shown Figure 2.7(a). The function generator is a source of excitation signals. The excitation current with a power amplifier is arranged from an excitation coil and a magnetizer of the UEC probe. Meanwhile, the detection signal generated by the detector coil is quite weak. In order to obtain a measurement signal with a high signal to noise (S/N) ratio, the detection signal is amplified and filtered by amplifiers and filter circuits. Finally, the voltage and phase signals are measured to evaluate flaws using a phase lock-in amplifier device. For the sensing process in all surface areas of the test piece, a robot device is required to precisely arrange the displacement position of the probe.

The systems on the rotating UEC probe have the same devices as in the one-direction UEC probe, such as a function generator, a pair of power amplifiers, an amplifier with filter, and a probe with a combination of two excitation coils and a detector coil, arranged as shown Figure 2.7(b). A phase shifter is used to create the 90° phase difference, and two excitation currents supply excitation coil #1 and excitation coil #2, which induce rotating eddy currents[3, 9].

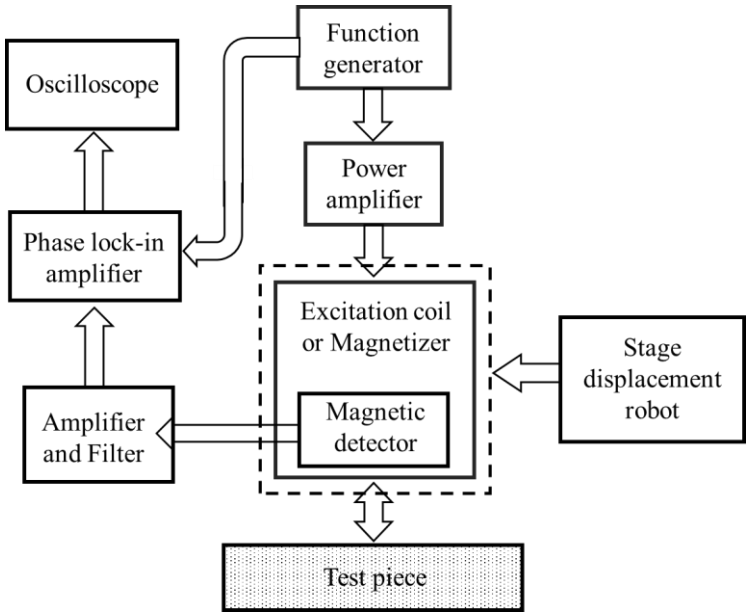

(a)

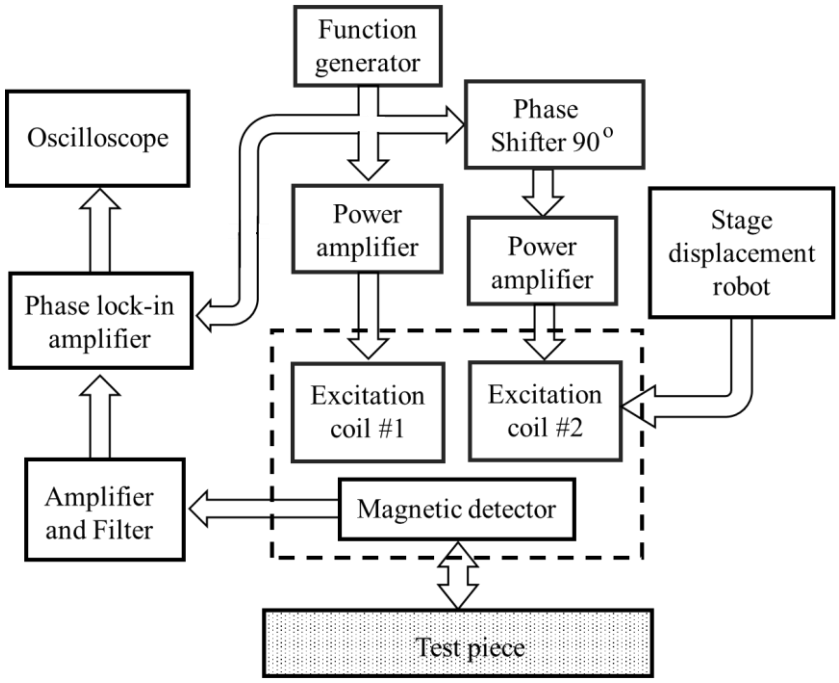

(b)

Figure 2.7 Apparatus of the UEC system. (a) One-direction UEC system. (b) Rotating UEC system.

2.7. UEC Probe Design Models

The following sections will briefly present various UEC probe models that have developed from the one-direction UEC probes and the rotating UEC probes.

2.7.1. One-Direction UEC Probes

2.7.1.1. One-Direction Hoshi Probe

The One-Direction Hoshi (ODH) probe is the first UEC by Hoshikawa and Koyama. The probe is included as separate coil probe with single frequency exciter. It consists of a large size of rectangular excitation coil in tangential orientation, and a small circular detector coil, in pancake orientation whose position is in the lower middle of the excitation, as shown in Figure 2.8. The ODH probe is designed to be able to detect flaws like cracks in the weld zone, or the rough surface test piece of nonmagnetic stainless steel and the edge of the piece. Besides that, it was able to eliminate the effect of lift-off noise. [22, 23]. The unique element proposed from the design of this probe is a detector coil that has self-differential and self-nulling properties, so that it can eliminate the need for a bridge for balancing.

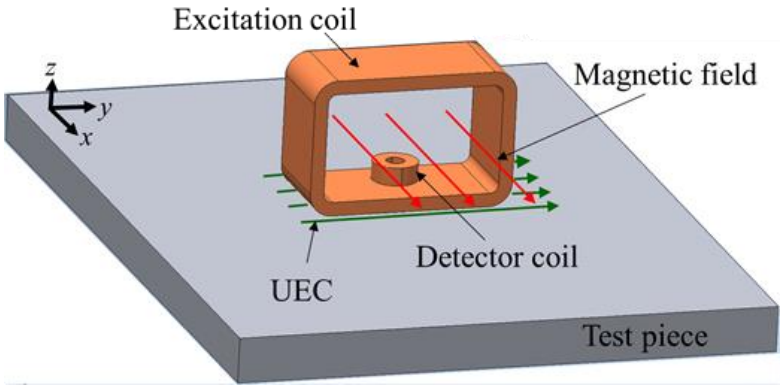

Figure 2.8 The structure of the One-Direction Hoshi probe.

In the absence of flaws in the test piece, the detector coil with its self-differential and self-nulling properties will keep the ε at zero, as shown in Figure 2.9(a). When there is a flaw, eddy currents are in disorder due to the flaw and cause the opposite magnetic field to become distorted. This situation is captured by the detector coil as an unbalanced condition, where $\varepsilon_1 \neq \varepsilon_2$. Therefore, ε appears as a representation of the flaw, as shown in Figure 2.9(b).

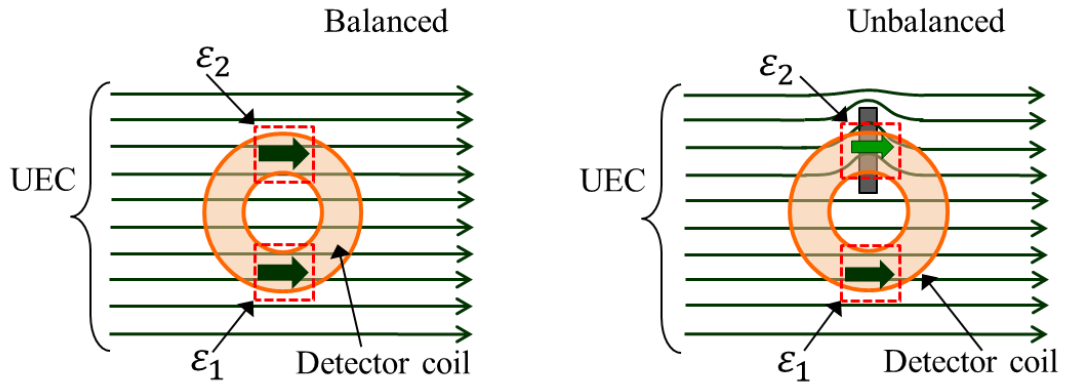

Figure 2.9 EMFs conditions are balanced (a) and unbalanced (b) due to the presence of a flaw.

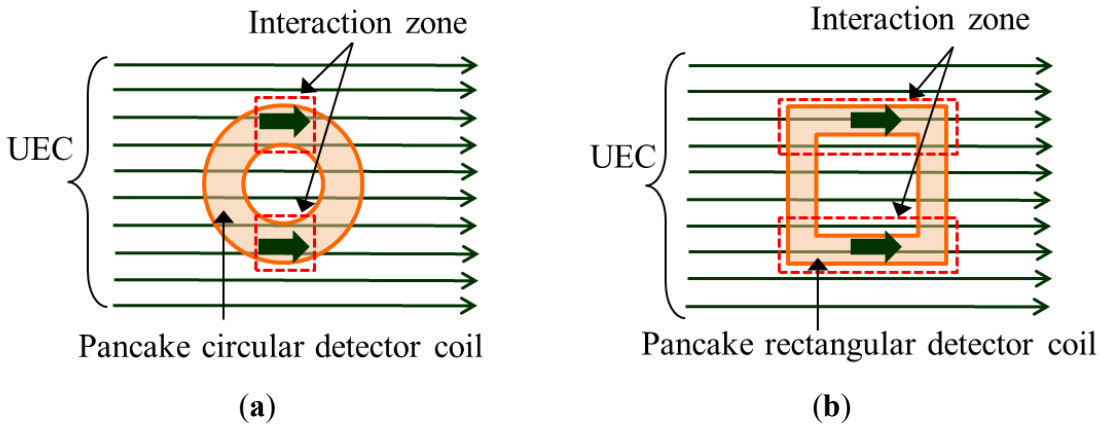

Figure 2.10 Interaction zone of the detector coils. (a) Interaction zone on the pancake circular detector coil. (b) Interaction zone on the pancake rectangular detector coil.

One critical factor for increasing sensitivity is to enlarge the interaction zone

between the detector coil and the capture area of the opposing magnetic field [23-25]. The study was carried out by Hoshikawa on the two forms of detector coils, namely circular and rectangular detector coils, as shown in Figure 2.10. Both show good performance, withstanding lift-off noise. However, the rectangular detector shows a larger detection signal compared to a circular one, since a rectangular detector coil has larger interaction zone than a circular detector coil.

2.7.1.2. Cross Probe

Another type of tangential probe design is the cross probe (CP). The idea of developing this probe is to obtain a probe with better capability to S/N by reducing noise [26, 27]. The probe is composed of a tangential excitation coil and a tangential detector coil that are crossed to each other, as shown in Figure 2.11.

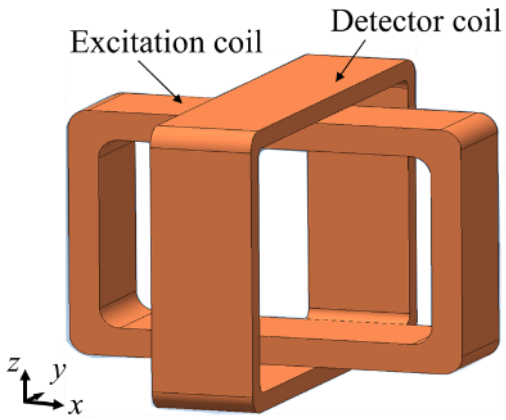

Figure 2.11 The structure of cross probe.

In the test piece condition without flaws, when the energy excitation coil induces a uniform eddy current on the surface of the test piece, the direction of this current is perpendicular to the detecting coil. Therefore, the EMFs does not appear in part of the detecting coil, as shown in the Figure 2.12.

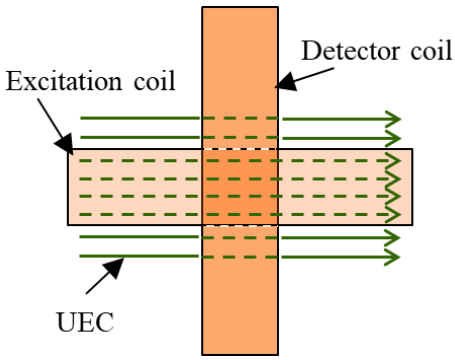

Figure 2.12 The eddy current flows under a cross probe without a flaw.

Furthermore, when the test piece contains a flaw and then eddy current inducted around the flaw, there is a part of the current to be distorted. This current becomes parallel with the direction of the wire turn of the detection coil, as shown in figure 2.13(a). This situation causes the opposing magnetic field arising from this eddy current generates an electromotive force in the area of the coil above it. So, the detection signal appears.

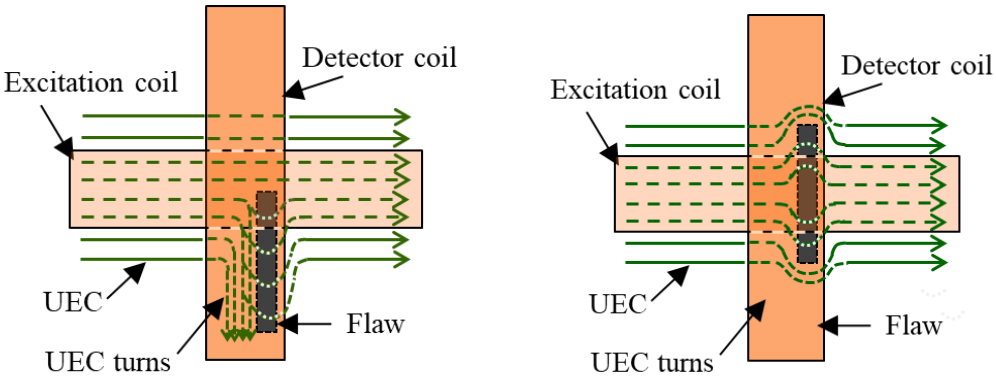

(a) **(b)**

Figure 2.13 The eddy current flows under a cross probe, (a) with a flaw, (b) with a flaw in the middle of the detector coil.

For detector coil, it has large size with tangential geometry. This position produces minimal lift-off noise and can provide phase information as a representation of the flaw depth. This ability makes eddy current testing more reliable for quantitative detection of

deficiencies compared to conventional probes. When the existence of a transverse flaw is right in the middle of the probe, this situation generates two EMFs that are opposite polarity on the two sides of the detector coil and cancel out each other. The detection signal becomes zero. It described in Figure 2.13(b). This pattern shows that the detecting coil has self-differential and self-nulling characteristics. Although there is a variation signal from lift-off probe that causes small changes in amplitude but does not affect the direction of the eddy current circulation [26, 27].

Based on the research that has been done, shown the result that the flaw length significantly influences signal amplitude. The lift-off probe also affects the signal amplitude, but it has no significant effect on signal phase. This means the probe can be used to predict the depth of the flaws that is trusted.

2.7.1.3. Plus-Probe

The plus probe (PP) is one type of tangential eddy current probe. The purpose developed of the probe was to minimize lift-off noise and provides good phase signals as a representation of flaws depth. The probe arranged from an excitation coil and a pair of detector coils, and all the coils installed tangentially. detector coils position is orthogonal against the excitation coil, as shown in Figure 2.14.

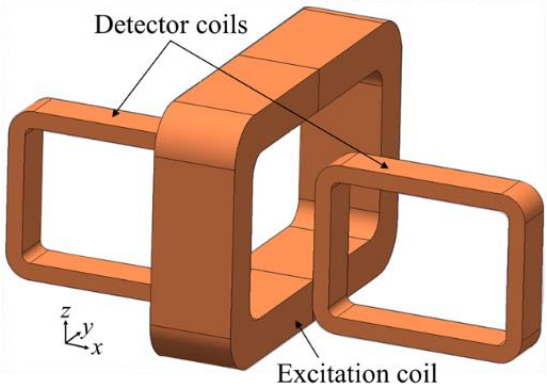

Figure 2.14 The structure of the plus probe.

The large detector coils make its interaction zone becomes larger and increases the S/N ratio of detection signals. Furthermore, the detection signals more immune to the lift-off effect [13, 28]. In principle, this probe is similar with a cross probe. The detecting coils only detect the magnetic field of eddy current parallel to the coil wire coil. When the test piece is flawless, the eddy current flowing perpendicular against the detection coil does not generate an electromotive force, as shown in figure 2.15.

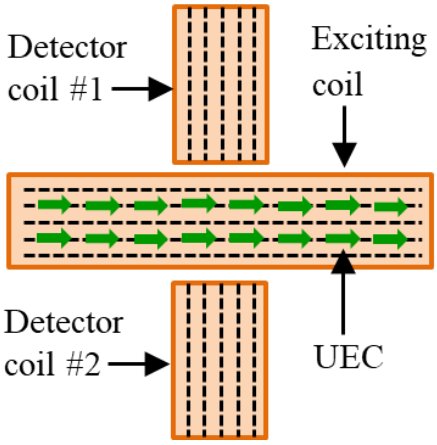

Figure 2.15 The eddy current flows under a plus probe without a flaw.

Furthermore, when the test piece contains transverse flaws that hind the eddy current flow, then there is a portion of the eddy current that turns and becomes parallel with the wire of the detection coil, as shown in Figure 2.16 (a). This condition causes the opposing magnetic field to arise and induces a part of the detection coil so that the electromotive force is generated and appears the detection signal.

However, the transverse flaw that its position is right in the middle under of the probe produces EMFs that cancel out each other. Therefore, the detection signal becomes zero, as illustrated in Figure 2.16(b). Detection conditions like this indicate that the probe has the characteristics of self-differential and self-nulling.

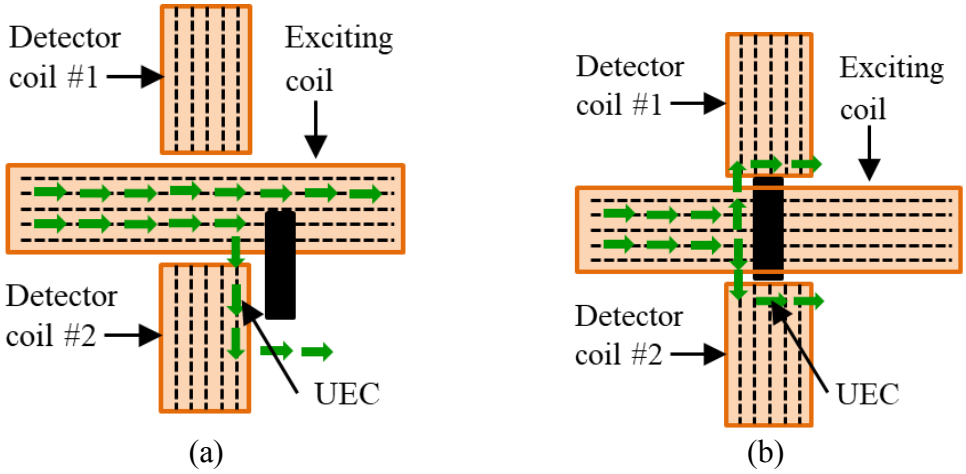

Figure 2.16 The eddy current flows under a plus probe, (a) with a flaw, (b) with a flaw in the middle under of the detector coil.

Hoshikawa gave a satisfying experimental result in which the PP probe provided a larger flaw signal magnitude, the signal to noise ratio being considerably more significant than that of a conventional probe. The exciting is the change in the depth of flaw that increases on the surface of the test material, significantly followed by also the increasing phase signal changes. Changes in the length of a flaw, with the same depth, did not cause a significant change of phase signal. Accordingly, the probe plus is promising to develop for the quantitative in evaluating flaws.

2.7.1.4. UEC Probe with a Giant-Magnetoresistance Detector

Basically, the excitation coil of a UEC probe with a giant-magnetoresistance (GMR) detector is the same as the Hoshi probe. However, the detection coil uses GMR components. as shown in Figure 2.17. GMR is set so that it will detect flaws whose length is parallel to the direction of eddy currents.

The GMR can work on low excitation frequency, under 1 kHz. Therefore, this probe has a deep skin effect, and this is its advantage. This probe is allowed to detect subsurface flaws [9,29,30,31]. In addition, a GMR with high sensitivity makes it effective for

detecting flaws like cracks on aluminum test piece [32].

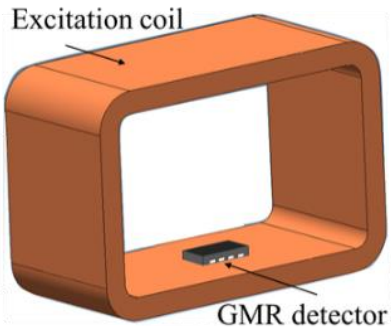

Figure 2.17 The structure of a tangential rectangle UEC probe with a GMR detector.

2.7.1.5. U-Shape ACFM Probe

The ACFM was developed by a researcher of the University College of London for detecting cracks in underwater environments [7]. The configuration of the ACFM probe is shown in Figure 2.18. It has a magnetizer and a combination of a tangential rectangular detector coil to measure the magnetic flux density in the x direction (*Bx*), and a pancake rectangular detector coil to measure the magnetic flux density in the z direction (*Bz*) with a cubic ferrite core. The flow of the induced UEC due to the probe is perpendicular to the flow of the magnetic field on the surface of the test piece.

The detector coils simultaneously measure *Bx* and *Bz* at the same position. When there are no flaws in the surface of the test piece, the signals measured with the coils have a constant value. However, if there is a flaw, the *Bx* signal shows two peaks due to a high intensity of UEC at the edges of the flaw. Meanwhile, the *Bz* signal indicates a sunken area that demonstrates the depth of the flaw [18].

The probe can detect flaws like cracks even from through the protective paint and the coating on the surface of the test piece of steel. Since the operators are not required to carry out surface cleaning, it reduces the inspection time. The ACFM probe can also be

applied to a test piece with a high temperature [5,6,14].

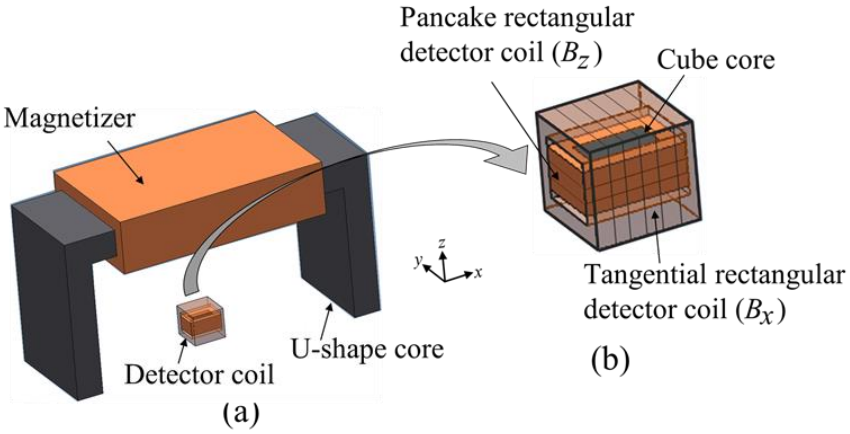

Figure 2.18 The structure of the one-direction ACFM probe, (a) One-direction ACFM probe. (b) Detector coil is a combination of tangential rectangular detector coil *Bx* and pancake rectangular detector coil *Bz*.

2.7.1.6. One directional Planar Probe

Planar coils are new in the design of probes, and have advantages such not creating heat, low leakage inductance, flexible substrate material, and being cheap in terms of production compared to other conventional applications. They also present increased immunity to the lift-off effect, and enhanced sensitivity [33-35].

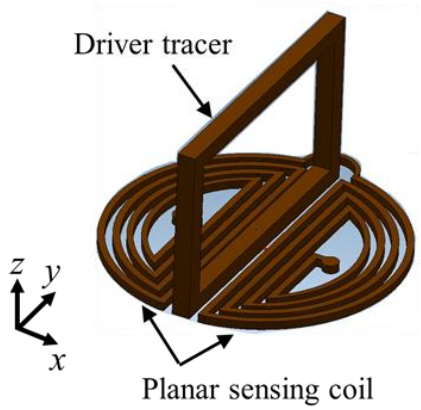

Figure 2.19 Structure of the one-drive planar probe.

The planar probe consists of an excitation coil, which is termed the driver trace, in the form of a tangential rectangle excitation coil and a pair of semicircular planar spirals as pancake detector coils, as shown in Figure 2.19. This detector coils have differential outputs with two symmetrical sensing coils. A planar probe produces a kind of spiral path on substrate material, with photolithographic processing.

Based on the configuration, the planar probes, when there is no flaw, show symmetric EMFs in both detector coils that differ in polarity and cancel each other out. The EMFs planar detector is zero. It is also self-nulling. When there are flaws, the detector becomes unbalanced. Therefore, the EMFs appears as a flaw representation that will increase with the increasing length of the flaw. The probe can reduce the influence of the lift-off effect and have high sensitivity, as well as an increase in the the S/N ratio, as reported in other research [36-38]. The probe can be used on a test piece surface that has an angle or is uneven [39]. The operation of the probe is designed to detect flaws like cracks of around 50 μm to 500 μm on the surface of the aluminum test piece of friction stir welding (FSW) joints [40].

2.7.1.7. Theta Probe

Theta probe designed having high detection capabilities, good phase signals and reduce the appearance of lift-off noise. The probe consists of a pancake circular excitation coil and a tangential rectangular detector coil. It has stronger induction and no lift off noise, as reported in other research [41] and as shown in Figure 2.20. It is different from the general configuration of a UEC excitation probe, however, the probe has similar properties to a tangential rectangular coil, which is the same shape as a detector coil. In the configuration, the detector coil only responds to the magnetic field due to flaws like cracks, and it resists lift-off variation, resulting in a high S/N ratio.

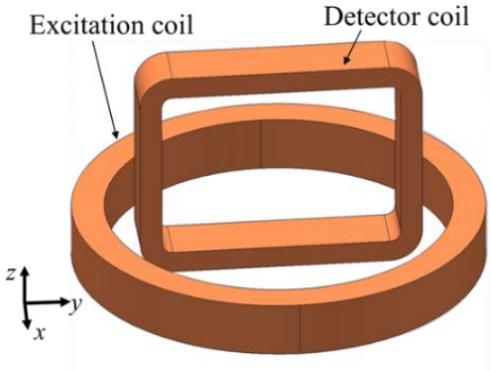

Figure 2.20 The structure of the theta probe.

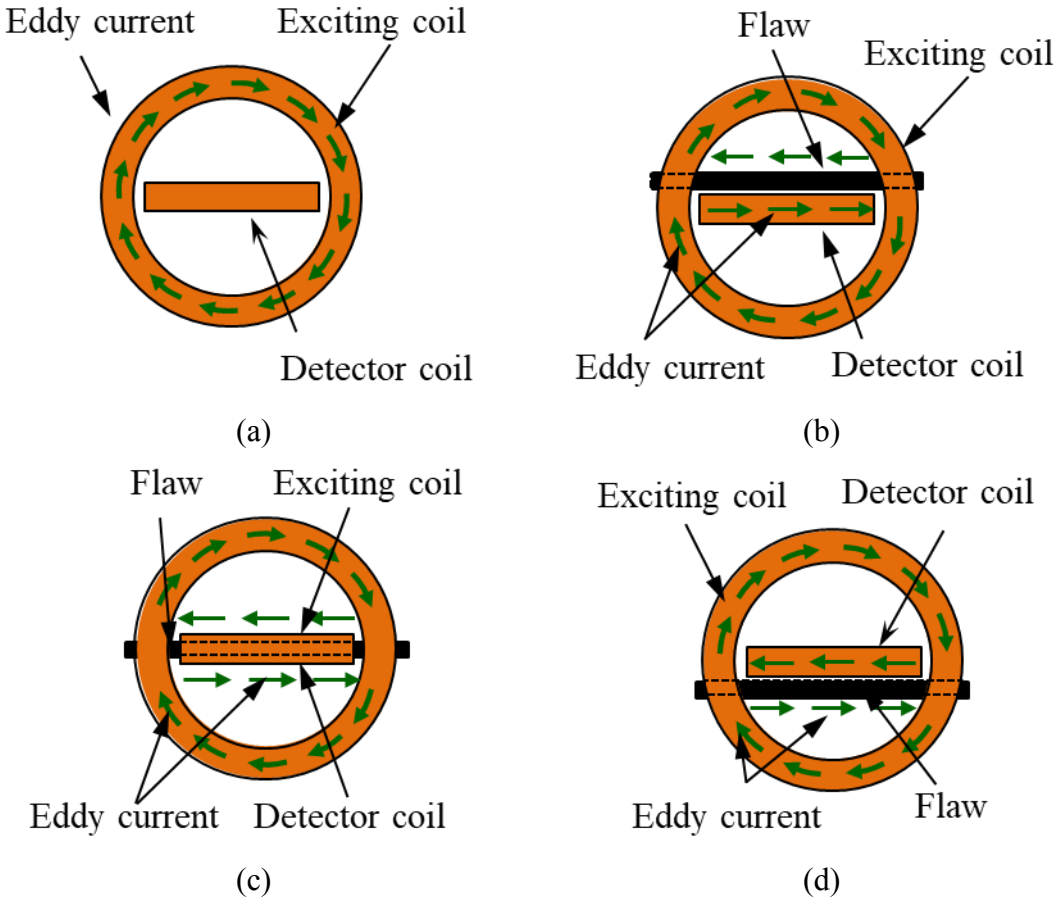

Figure 2.21 Eddy current circulation under theta probe, (a) no flaw, (b) with a flaw (plus signal), (c) with a flaw (no signal), (d) with a flaw (minus signal).

Pancake orientation is adopted to get strong induction. Under normal conditions, the eddy current makes circulation on the surface of the test piece rotates following the excitation coil shape. This pattern happens if there is no flaw, as shown in Figure 2.21 (a).

Furthermore, if the surface of the piece contains a flaw that transverse in the diameter of the excitation coil, the eddy current circulation will split in half to form a half-circle as shown in Figure 2.21(b)-(d).

The detector coil will generate a detection signal when its position beside the flaw, as in Figure 2.21(b) and (d). However, if the detector is right in the middle of the flaw, like as Figure 2.21(c), no detection signal resulted. This condition occurs, because the EMFs generated on the detector coil are opposite, and hence eliminates each other. The detector coil balances with the self-nulling nature [42]. Because of the probe generates minimal lift-off noise, then it does not influence much to the flaw signal. The phase signal able to be used for evaluating the depth of surface flaws. Theta probe able to uses as a quantitative measurement.

2.7.2. Rotating UEC Probe

2.7.2.1. Hoshi Probe with rotating UEC

The Hoshi Probe with rotating UEC (HPRUEC) was one of the first draft UEC investigations with its features; self-nulling, self-differential, free-off noise, and able to generates detection signals from flaws with different directional positions. The configuration of a HPRUEC consists of a pair of tangential rectangular excitation coils arranged orthogonal to each other and shaped like a cube, and a small pancake circular detector coil positioned at the center bottom of the excitation coil [43], as shown in Figure 2.22.

The rotating UEC is the resultant UEC (RUEC) of the *UECs* generated by excitation coil one and excitation coil 2 with two excitation currents which have 90° phase difference, as shown in Figure 2.23. UEC_1 and UEC_2 are *UECs* which are generated by excitation coil #1 and excitation coil #2, respectively.

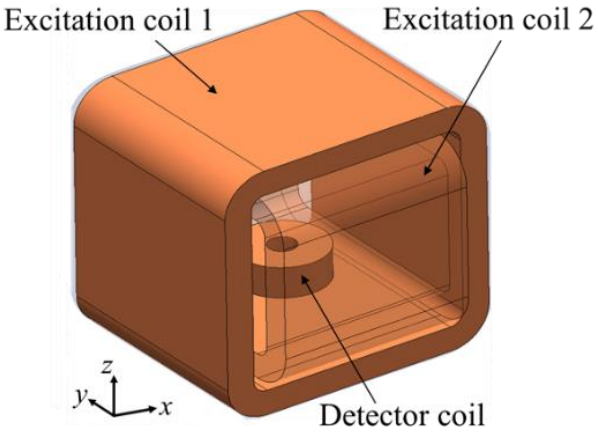

Figure 2.22 Structure of the HPRUEC.

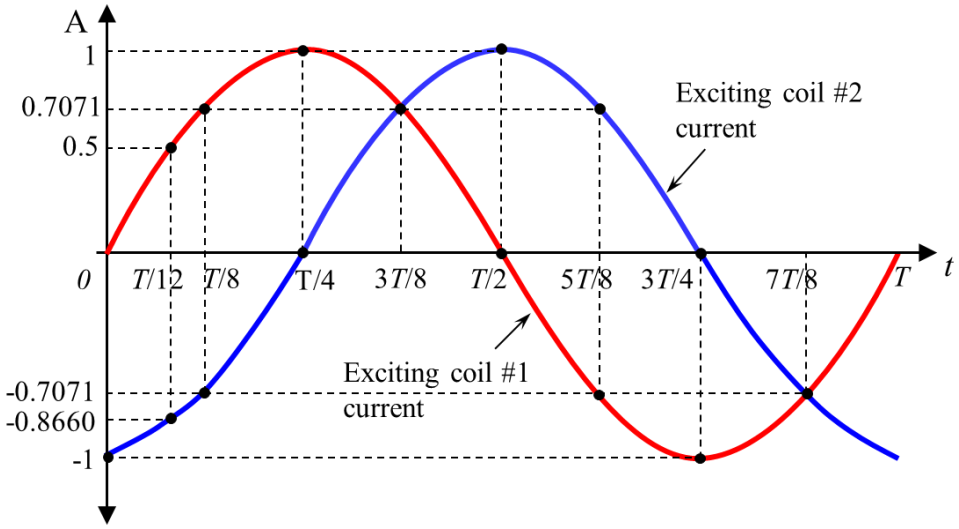

Figure 2.23 Two excitation currents which have 90° phase difference.

Both of *UEC*s shown in the equation (2.25) and (2.26). Where T is the period of the excitation current and A is the amplitude of the *UECs*.

$$UEC_1 = A\ sin\left({}^{2\pi t}/_{T}\right) \tag{2.25}$$

$$UEC_2 = A\ sin\left({}^{2\pi t}/_{T}\right) + {}^{\pi}/_{2} \tag{2.26}$$

$$RUEC = \sqrt{(UEC_1)^2 + (UEC_2)^2} \tag{2.27}$$

The two excitation coils are orthogonally installed. Therefore, it is assumed that

UEC_1 generated from excitation coil #1 flows to x direction, and UEC_2 generated from excitation coil #2 flows to y direction, as shown in Figure 2.24.

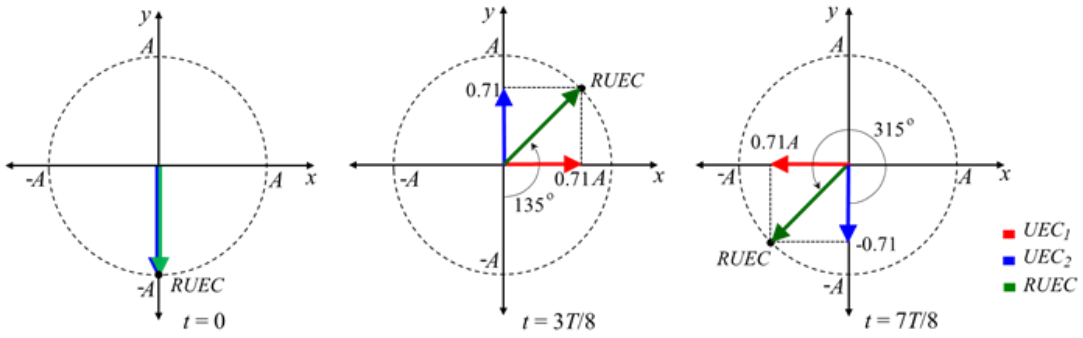

Figure 2.24 The resultant of the rotating *UEC* is formed by UEC_1 and UEC_2.

When two excitation currents are flowing in one period, *RUEC* is rotated in all directions with constant amplitude, following equation (2.27) [44]. Hence, the UEC distribution moves in rotating, as shown in Figure 2.25 [14, 17].

The generation principles of the EMFs of pancake circular detector coils with flaws and without flaws are the same as that of a one-direction UEC probe. The rotating UEC probe can detect flaws in all directions on surface of test piece of steel.

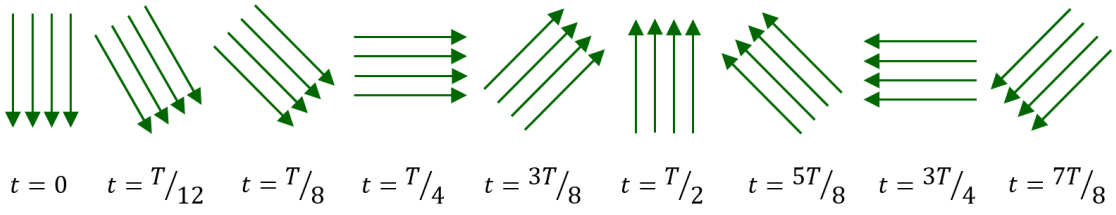

Figure 2.25 Movement of rotating UEC.

.

Besides, since the rotating UEC allows the flow of eddy currents always in a position perpendicular to the length of the flaw, then the EMFs will appear optimally. This high sensitivity is one of the main advantages of the probe. However, because to detect a

location point requires a cycle time for rotation, the scanning time of the probe with rotating UEC slower than the one-directional butterfly probe.

2.7.2.2. ACFM Probe with Rotating Eddy Current

The configuration of the ACFM Probe with Rotating Eddy Current (ACFMREC) is two magnetizers which are arranged orthogonally to each other, as shown in Figure 2.26, and a combination of two detector coils for B_x and B_z, which are the same as the detectors of a one-direction ACFM probe. The two excitation currents for each coil have the same amplitude and a single frequency but different in phases 90°. The generation of the rotating UEC of ACFMREC is same as that of a rotating UEC probe.

The detection principle of flaws with detector coils is the same with that of a one-direction ACFM probe. The advantages and disadvantages are the same as those of the rotating UEC [7,43]. The development of the ACFMREC is focused on the use of defect detection for steel in underwater environments [5,65].

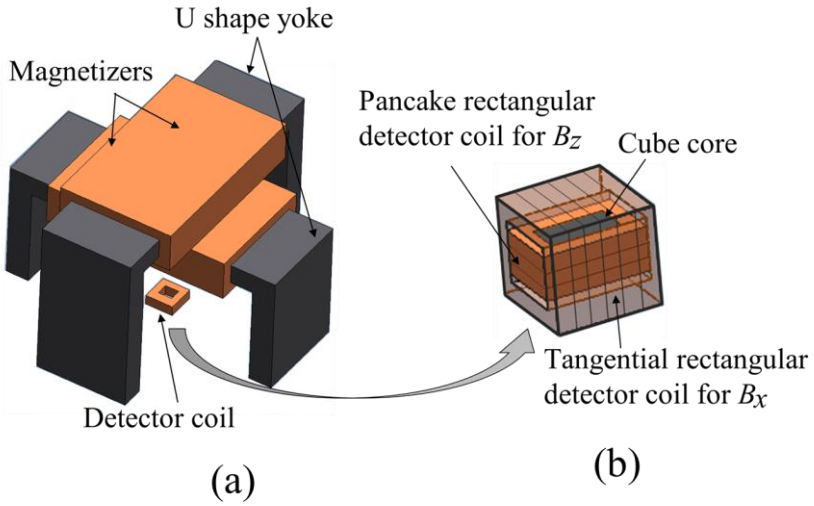

Figure 2.26 Structure of the ACFM probe with rotating UEC, (a) Magnetizer of ACFM probe, (b) Detector coil of ACFM is a combination of tangential rectangular coil for B_x and pancake rectangular coil for B_z.

2.7.2.3. Dual Driver Planar Probe

The disadvantage of the one directional planar probe is its incapability to detect flaws when the probe moves perpendicular towards the excitation coil or drive tracer, as reported in other research [40,45]. For this reason, a dual driver planar probe or Ionic+ Probe was developed. In the configuration, there are four parts of the drive tracer which ware made like rectangular excitation coil under tangential position, as shown in Figure 2.27. The four driver tracers (DT) are grouped into two parts, namely the DT horizontal and DT vertical. Each group is connected in series and supplied separately, so that each can set different excitation current amplitudes and phases. The detector coils are separated into four sections, which occupy four positions of the quadrant. All of the coils are pancake oriented. The four parts are connected in series into one unit with the connection of terminal pairs 2–3, 4–5, and 6–7. The output from the connection of terminal pairs 1–8 is differential, which is the total output of the detector coils. This new probe is also known as the Ionic + probe.

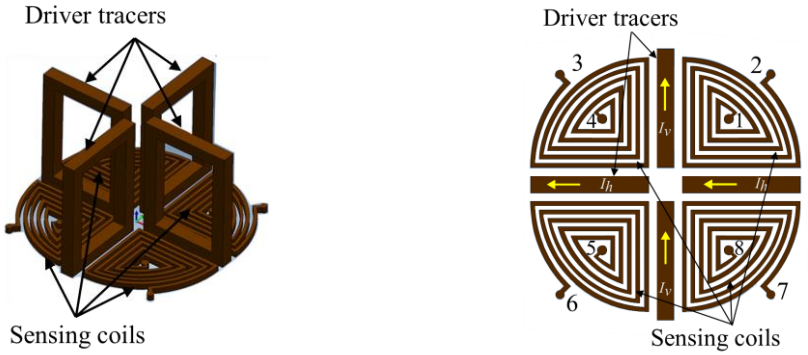

(a) Side view (b) Top view

Figure 2.27 Structure of Dual Driver Planar Probe, (a) Side view, (b) Top view.

The probe can detect flaws like cracks in all directions on test piece of aluminum. In addition, the proper flow of the UEC against a flaw is generated by the setting of the

excitation current amplitude and phase for each excitation coil, enhancing the sensitivity of flaw detection [36,46].

2.8. Summary

Studies on the Uniform Eddy Current Configuration Probe (UEC) configuration provide an understanding of the characteristics that emerge from the design of the probe model. There are two factors that indicate the effect in increasing the sensitivity of a UEC probe design.

1. The first factor is the configuration of the excitation coil and the detection coil. UEC probe configurations must be developed so that the excitation coil and detection coil produce higher induction current densities and cause an increase in electromotive force in response to flaws.
2. The second factor is the shape and orientation of the detector coil. The self-differential and self-nulling natures of the detector coil should be considered. That is, the shape and orientation of the detector coils should be determined, whether in the shape of a single coil or it is built from two or several coils.

Hereafter, in Table 2.1 and Table 2.2 are summarize of the models of UEC probes that have presented.

Table 2.1 Summary of the comparison of the models of one-direction UEC probes.

Models and Configurations	**Characteristic**
UEC probe (Hoshi probe) **Excitation;** One tangential rectangular coil.	• The probe has self-differential and self-nulling properties and is immune to the lift-off. • The probe can detect the flaw on the weld zone surface and edge of the test piece and can provide phase signal as information of flaw depth.

Detector; One pancake circular coil	• The probe relatively has a weak induction and a small detection signal. • The probe can't detect the direction of flaw length that is parallel to the direction of UEC flow.
Cross probe **Excitation;** One tangential rectangular coil **Detector;** One tangential rectangular coil	• The probe has self-differential and self-nulling properties and is immune to the lift-off. • The probe can detect the flaw on the weld zone surface and can provide phase signal as information of flaw depth. • The probe relatively has a weak induction and a moderate detection signal. • The probe can't detect the direction of flaw length that is parallel to the direction of UEC flow.
The plus- probe **Excitation;** One tangential rectangular coil **Detector;** Two tangential rectangular coils	• The probe has self-differential and self-nulling properties and is immune to the lift-off. • The probe can detect flaw on the weld zone surface and can provide phase signal as information of flaw depth. • The probe relatively has a weak induction, and a moderate detection signal. • The probe can't detect the direction of flaw length that is parallel to the direction of UEC flow. • The probe can't detect a short flaw that is less than the distance between the two detector coils, and the position right under the excitation coil.
UEC probe with a GMR detector **Excitation;** One tangential rectangular coil **Detector;** One GMR component	• The probe can detect the flaw on the weld zone surface and provides information of flaw depth. • GMR is high accurate. • The probe can work at low frequencies below 1 kHz so that, it can detect flaws deeper into the test piece. • The probe doesn’t have self-differential and self-nulling properties and is not immune to the lift-off.
U-shape ACFM probe **Excitation;** One magnetizer	• The probe relatively has strong induction and is immune to the lift-off. • The probe can detect the flaw through coating and the flaw on the weld zone surface.

Detector; One Combination of a tangential rectangular coil and a pancake rectangular coil	• The probe can provide information on the size and depth of flaw only from amplitude signal containing Bx and Bz components. • The probe can't detect the direction of flaw length that is parallel to the direction of UEC flow.
IOnic probe **Excitation;** One tangential rectangular coil **Detector;** Two pancake semicircular planar coils	• The probe has self-differential and self-nulling properties and is immune to the lift-off. • The probe has high sensitivity, and can detect the micro size flaw on the FSW zone surface • The probe can provide information of flaw depth • Probe production requires high precision in making symmetrical planar spiral detectors that must be precisely similar between the two sides.
Theta probe **Excitation;** One pancake circular coil **Detector;** One tangential rectangular coil	• The probe relatively has strong induction and is immune to the lift-off. • The probe can detect the flaw on the weld zone surface and can provide phase signal as information of flaw depth. • The probe can’t detect short flaw that is shorter than the diameter of the excitation coil. • The probe can't detect the direction of flaw length that is parallel to the direction of UEC flow.

Table 2.2 Summary of the comparison of the models of probe with rotating UEC.

Models and Configurations	**Characteristic**
Rotating UEC Hoshi probe **Excitation;** Two tangential rectangular coils **Detector;** One pancake circular coil	• The probe has self-differential and self-nulling properties and is immune to the lift-off. • The probe can detect flaw in all orientation on the weld zone surface and edge of the test piece. • The probe can provide phase signal as information of flaw depth. • The probe relatively has a weak induction and a small detection signal.

Rotating ACFM probe **Excitation;** Two magnetizers **Detector;** One combination of a tangential rectangular coil pancake rectangular coil and a	• The probe relatively provides strong induction and is immune to the lift-off. • The probe can detect flaw through coating, and detect flaw in all direction on the welding zone surface • The probe can provide information on the size and depth of flaw only from amplitude signal containing *Bx* and *Bz* components. • The probe is not recommended for small test objects.
Rotating dual driver planar probe or Ionic+ probe **Excitation;** Four tangential rectangular coils **Detector;** Four pancake quarter circular planar coils	• The probe has self-differential and self-nulling properties and is immune to the lift-off. • The probe has high sensitivity and can detect the micro size flaw in all direction on the FSW zone surface. • The probe can provide information of flaw depth. • The control of driver tracer currents and phase can maximize the detectability of flaw without the changes of the probe position. • Probe production requires high precision in making symmetrical planar spiral detectors that must be precisely similar between four sides.

Chapter 3
3. One Directional UEC Probe with A Pair Pancake Excitation Coil

3.1. Introduction

Based on their configurations, eddy current probes are generally classified into two types. First is the combined transmit–receive probe equipped with a single coil that functions as an excitation coil and a detection coil. The concept of this single coil is based on the principle that a change in impedance occurs when discontinuities disrupt the eddy current distribution in the test piece [12,47,48]. Another type of eddy current probe is the separate transmit–receive (STR) probe that has two distinct coils, one for excitation and another for detection. A unique model of the STR probe is the UEC probe. This probe has been developed to immune for the lift-off noise generated by the uneven surface of test materials, such as found in weld zones [23-49].

The nature of the UEC probe results from the self-differential properties possessed by its detector coil. The electromotive forces (EMS) generated on opposite parts of a detection coil are the same but have opposite polarities; accordingly, they cancel out each other. As a result, the output voltage, V_O of the coil is zero; this nature is called self-nulling [23,25,43,50]. Because the UEC probe reduces the effect of lift-off on the measurement

signal, the signal can be regarded as a reliable sizing information of the flaw [51,52]. However, because the excitation coil of the UEC probe is tangentially oriented, its signal is relatively small. In this configuration, not all parts of the detection coil contribute to induce the signal; only parts that are close and parallel to the test piece are actively involved in this regard. To overcome relatively small signals, several trials using excitation currents with high frequencies and amplifier circuits have been conducted [22,43,53,54].

In the present study, a new demand for eddy current testing is the ability of portable instruments that can detect flaws that are getting smaller and buried with a lower amplitude of excitation currents. Thus, the operational time of the probe can be longer. A probe with double excitation coils was used with a giant magnetoresistance sensor [20]. The configuration and shape of excitation and detection coils are designed to enhance the S/N ratio and power supply efficiency during measurement [21,22].

The proposed UEC probe consists of a pair of rectangular excitation coils and a circular detection coil; all coils are in a pancake orientation. The authors named the device as ‘butterfly probe’. The flaw detection principle involved in the butterfly probe is analysed with a finite element simulation. Its ability to detect flaws on the aluminium plate surface is discussed based on experimental results.

3.2 Material and Methods

3.2.1. Coils Structure of Butterfly Probe

To improve the detection capability of an eddy current probe, an essential factor is increasing the intensity of eddy currents generated by the probe. Accordingly, the butterfly probe has a pair of excitation coils with the same dimensions but wound in opposite directions; specifications are as shown in Figure 3.1. Each excitation coil

generates an eddy current that is opposite in circulation to the coil's winding direction. A circular detection coil is installed at the bottom and centre of the coils.

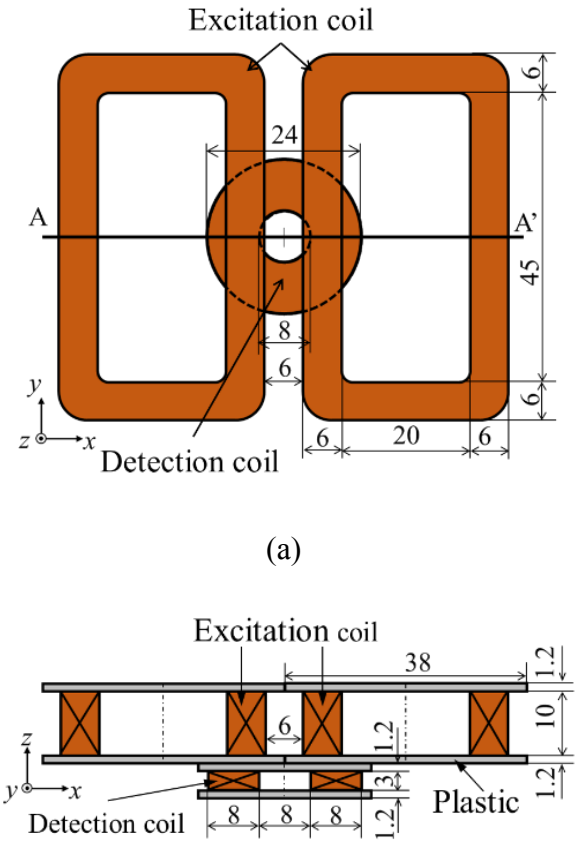

Figure 3.1 Structure of butterfly probe (unit in mm); the number of turns in each excitation coil is 1000: (a) Top view; (b) Section view of A-A'.

On the area with a blue dotted line shown in Figure 3.2, the eddy currents of the two coils merge and form UEC s with an intensity that is practically twice that of the eddy current from one coil.

There are two conditions of the butterfly probe; balanced and unbalanced conditions. These conditions are determined by the response of the interaction zone of the detection coil against the UEC, as shown by the red dotted line in Figure 3.2.

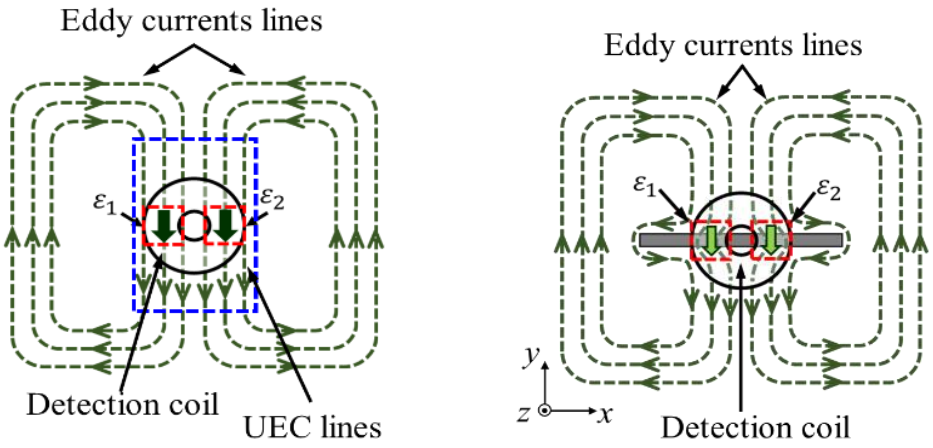

(a) (b)

Figure 3.2 Butterfly probe under balanced condition: (a) without flaw, (b) with flaw.

Under the balanced condition, EMFs ε_1 and ε_2 of the detection coil are of the same amplitude, but opposite in polarities; as a result, they cancel out each other. Consequently, the detection coil output is zero; a nature called self-nulling. as shown in Figure 3.2(a).

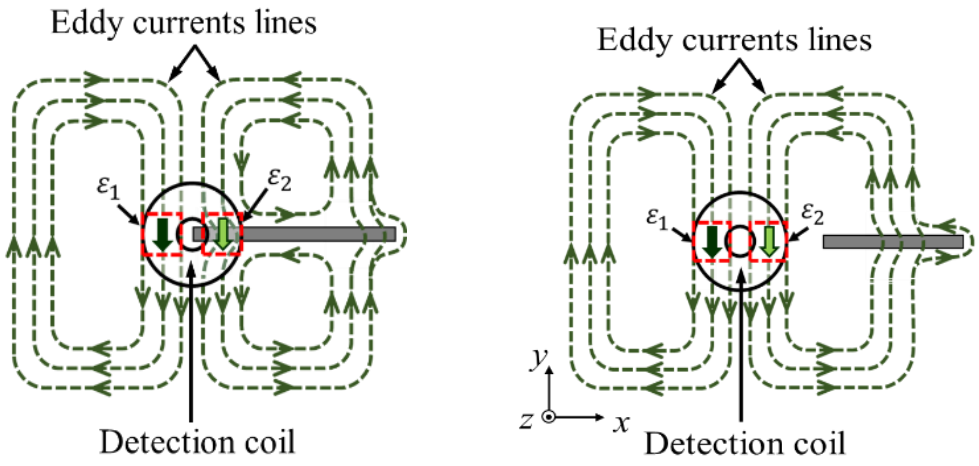

(a) (b)

Figure 3.3 Butterfly probe under unbalanced condition: (a) the edge of a flaw is located under the detection coil; (b) the flaw is located a short distance away from the detection coil.

The output is also zero when the probe is positioned in the middle of a flaw, as shown in

Figure 3.2(b); this is because the eddy currents have the same disturbance at two sides of the detection coil.

The unbalanced condition, as shown in Figure 3.3, is divided into two models. The first model, the edge of a flaw is located under the detection coil is shown in Figure 3.3(a). A Flaw causes disturbance UEC flowing. It causes the detection coil to appear to have unequal amplitudes and generates the voltage output.

The second model is a flaw located near to the detection coil and disrupts the circulation of UEC, as shown in Figure 3.3(b). The flaw causes ε_1 and ε_2 of the detection coil to have unequal amplitudes; this also results in generating output. As mentioned above, the middle of the probe is the most sensitive area for detecting flaws.

To achieve the best accuracy, the important factor for the butterfly probe is that the specifications of the two excitation coils should be the same. Moreover, the detection coil must be installed in such a position where self-nulling occurs.

3.2.2. Numerical calculations

To observe the distribution of eddy currents in the test pieces using the conventional UEC and butterfly probes, a time-harmonic analysis is implemented by employing a finite element analysis with Magnet 7 version 7.4.1 from Mentor Graphics Corporation located in Wilsonville, Oregon USA, which used the current vector potential (T), the magnetic scalar potential (Ω) method was used. In conducting medium, the basic equations of the method are expressed by using Faraday's law, Ampere's law and constitutive relation:

$$\nabla \times E = -\frac{\partial B}{\partial t} \tag{3.1}$$

$$B = \mu H \tag{3.2}$$

$$E = \left(\sigma + \varepsilon \frac{\partial}{\partial t} \right)^{-1} \cdot J \tag{31}$$

$$J = \nabla \times H \tag{3.4}$$

$$J = \sigma E + \varepsilon \frac{\partial E}{\partial t} \tag{3.5}$$

where the various quantities involved are defined as,

E: Electric field intensity (V/m)

H: Magnetic field intensity (A/m)

B: Magnetic flux density (T)

J: Current density (A/m^2)

t: Time (s)

ε: Material permittivity (F/m)

σ: Material conductivity (S/m)

μ: Magnetic permeability (H/m)

We then have the following equation by using Equations (5) to (8):

$$\nabla \times \left[\left(\sigma + \varepsilon \frac{\partial}{\partial t} \right)^{-1} \cdot \nabla \times H \right] + \mu \frac{\partial H}{\partial t} = 0 \tag{3.6}$$

The software is used together with Equations (3.5) and (3.6).

The element of the mesh was modeled as a linear superposition of polynomial basis function for high accuracy. The total number of meshes was 947,420. The analysis was carried out with the meshes of the butterfly probe and the area under the probe as small a size as possible within the performance of a personal computer.

Figure 3.4 shows the analytical model set up of the butterfly probe. The size and configuration of the rotating UEC probe were the same as those shown in Figures 3.1 and

3.5. In the analytical model, an aluminum plate test piece was modeled with dimensions of 120 mm in width, 120 mm in length, and 10 mm in thickness.

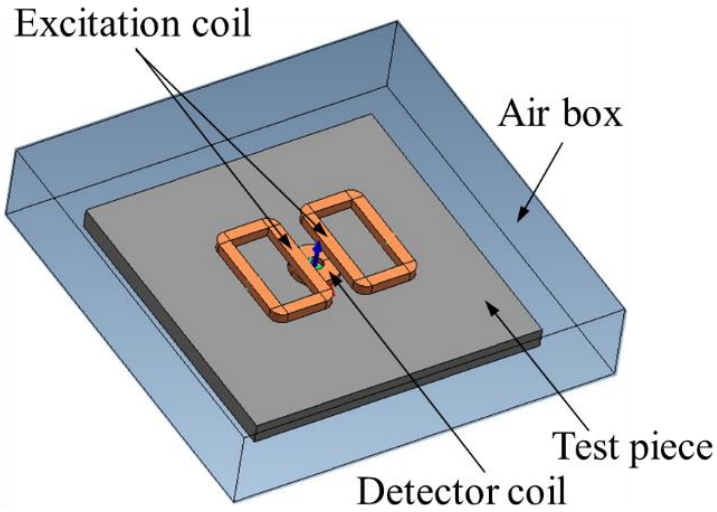

Figure 3.4 The analytical model set up of the butterfly probe.

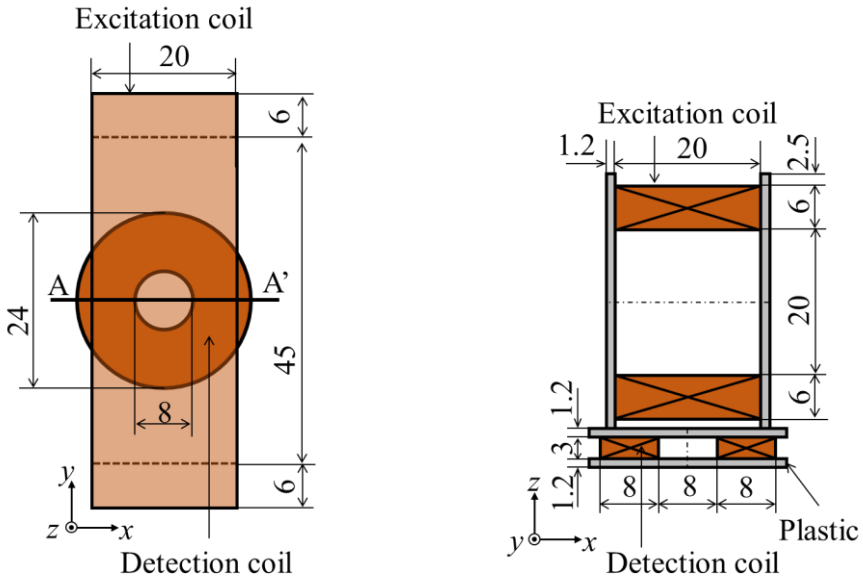

Figure 3.5 Coil structure of conventional UEC probe (unit in mm). The number of turns of an excitation coil is 2000. (a) Bottom view (b) Section view of A-A'.

The electromagnetic parameters used in the analysis are listed in Table 3.1. The excitation frequency and current for both probes are10 kHz and 6 mA, respectively.

Table 3.1 Electromagnetic parameters used in butterfly probe analysis.

Parameters	**Aluminium test piece**	**Copper wire of coil**
Electrical conductivity, σ	35 MS/m	57.7 MS/m
Relative permeability, μ	1	1

The analytical results are shown in Figure 3.6. In Figure 3.6(a), the amplitudes of the eddy currents of J_1 and J_2 generated by each excitation coil of the butterfly probe are practically the same. Moreover, the induction, J_{total}, which is a UEC produced by both coils, is twice larger than J_1 (or J_2). Meanwhile, the analytical results of conventional UEC probes as shown in Figure 3.6 (b), the eddy current J_c is smaller, even though the number of turns is equal to the number of coil excitation windings on the butterfly probe.

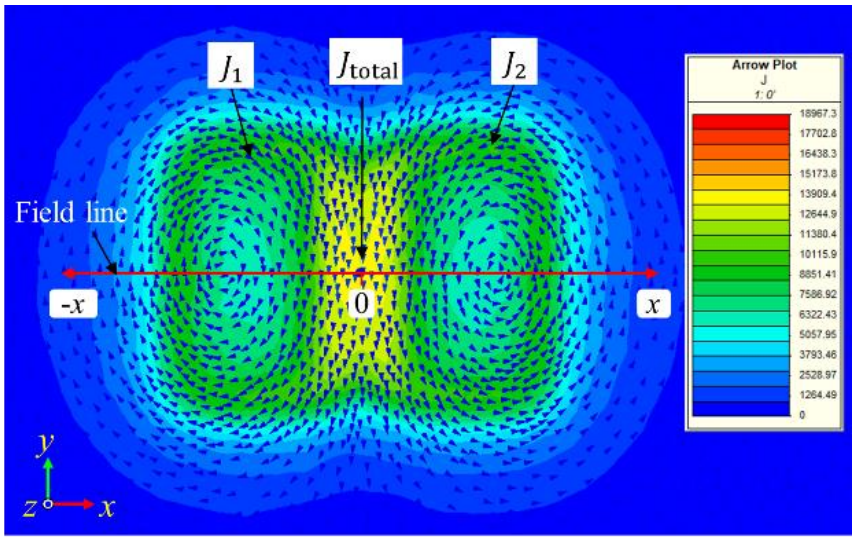

(a)

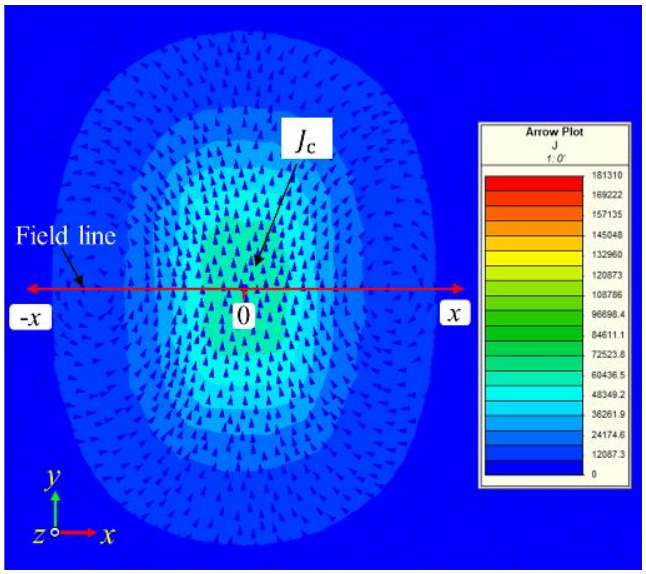

(b)

Figure 3.6 Arrow plot of eddy current distribution on the surface of aluminium test piece using (a) Butterfly probe; (b) Conventional UEC probe.

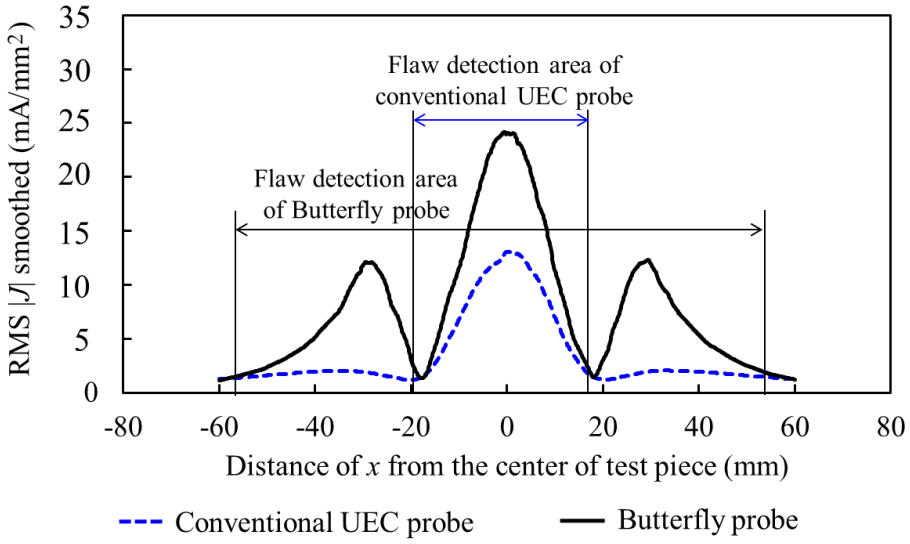

Figure 3.7 Eddy current density in the *x*-direction on the surface of the aluminium test piece using Butterfly and Conventional UEC probes.

For this reason, only the bottom surface part of the excitation coil of the conventional UEC probe mainly contributes to inducing the eddy currents. Figure 3.7 is the density of

eddy currents are measured along red line *x* shown in Figure 3.6.

The eddy current density that is generated using the conventional UEC probe indicates only one amplitude peak. Meanwhile, the eddy current density generated using the butterfly probe indicates three peaks. The highest peak density is in the middle of the probe axis, where the peak produced by the butterfly probe is approximately 1.8 times higher than the peak produced from a conventional UEC probe. Besides, the width of the eddy current density is broader than the density produced by conventional UEC probes. Therefore, the detection area of the butterfly probe is three times wider than conventional UEC probes.

3.3. Experimental Setup

Aluminium plate 5052 used as the test plate; on its surface, there were four artificial flaws whose sizes listed in Table 3.3; their positions are shown in Figure 3.8.

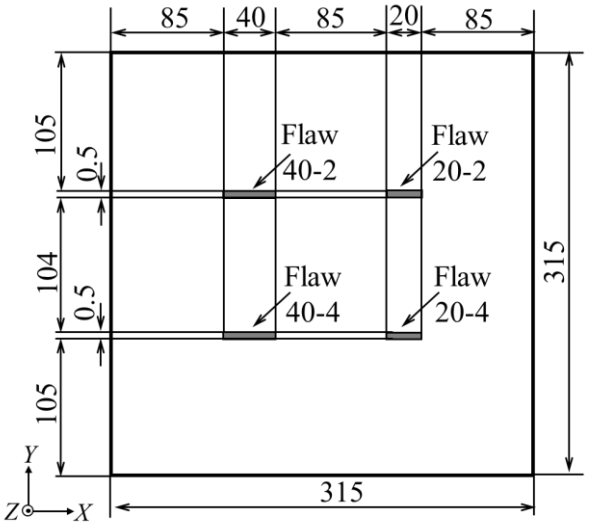

Figure 3.8 Aluminium test piece dimension for experiment (unit in mm).

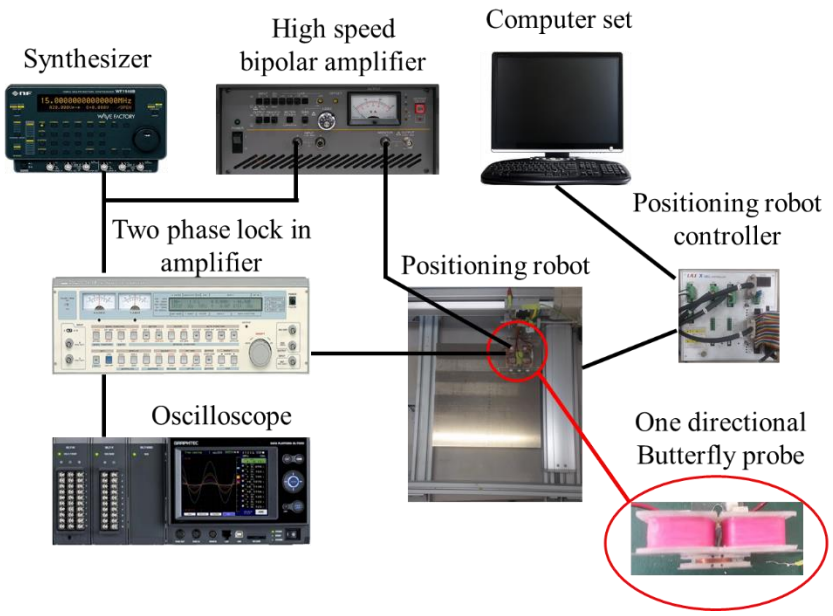

Figure 3.9 Experimental set-up for Butterfly probe testing.

The experimental setup is shown in Figure 3.9. The specifications of the coils summarised in Table 3.2. The excitation signal was the sine wave with frequency 10-kHz that generated by a function generator (WAVETEK). Furthermore, the signal was amplified to 6 mA with a high-speed bipolar amplifier (NF HAS 4012).

In experiments, excitation for butterfly probes and conventional UEC probes was conditioned the same at an excitation current of 6 mA. Next, the voltage of the excitation related to power consumption observed.

3.3.1. Specification of Coils and Test piece

Specification of Butterfly probe coils are shown in Table 3.2. Furthermore, the specification of the test piece with artificial flaw is given in Table 3.3. The signal from the detection coil is processed with a two-phase lock-in amplifier (NF 5601B) and stored in a digital oscilloscope (Graphtec GL7000) with a 4-Hz data sampling capacity. To move the butterfly probe over the scanning surface of the test piece, a computer-controlled

positioning robot module is used; the robot speed is 10 mm/s. The scanning interval is 2.5 mm in the *x*-direction and 2.5 mm in the *y*-direction. The clearance between the probe and aluminium plate surface is approximately 2 mm.

Table 3.2 Specifications of coils of Butterfly probe.

Component		**Specification**	
Butterfly probe	A pair-Excitation coil	Wire diameter	0.2 mm
		Turns	2×1000
		Resistance	240 Ω
		Inductance	87.8 mH
		Impedance	5.51 kΩ
	Detection coil	Wire diameter	0.2 mm
		Turns	330
		Resistance	16.2 Ω
		Inductance	1.42 mH
		Impedance	91.0 Ω

Table 3.3 Size of flaws on test piece surface.

Symbol of Flaw	**Width (mm)**	**Length (mm)**	**Depth (mm)**
20-2	0.5	20	2
20-4			4
40-2		40	2
20-4			4

3.3.2. Scanning Direction for Butterfly Probe

The butterfly probe has two scanning directions, as shown in Figure 3.10. Scanning #1 is perpendicular to the sensitive axis of the excitation coil; scanning #2 is parallel to the sensitive axis of this coil.

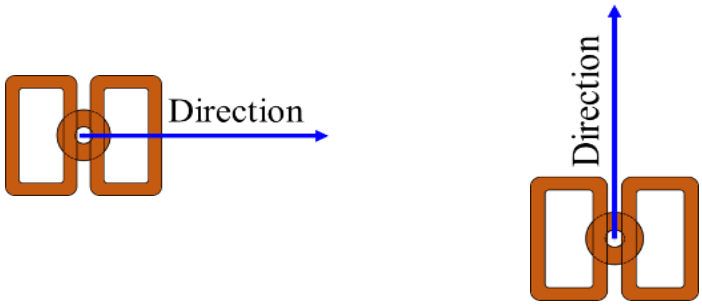

(a) (b)

Figure 3.10 The Scanning directions of butterfly probe: (a) Scanning #1; (b) Scanning #2.

The focus of observation from this scan direction is the axis position of the probe excitation coil to the length of the flaw, whether its position is perpendicular or parallel, which consequently results in the detection signal.

3.4. Results and discussion

The scanning area and paths on the test piece shows in Figure 3.10. In scanning #1, the butterfly probe moves in the *x*-direction and shifts in the *y*-direction, then repeated until the scanning covers all the flaws. Following, scanning #2 is the opposite of scanning #1. The probe moves in the *y* direction and shifts in the *x* direction.

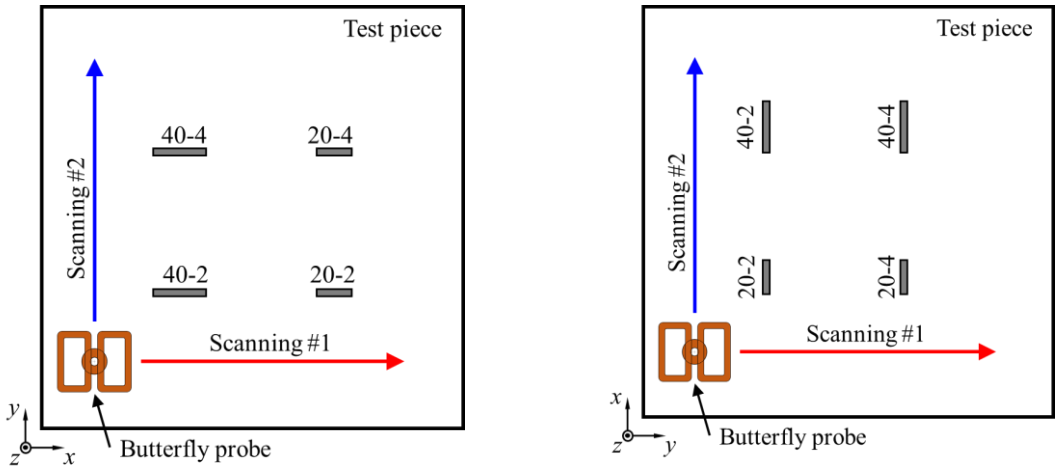

(a) (b)

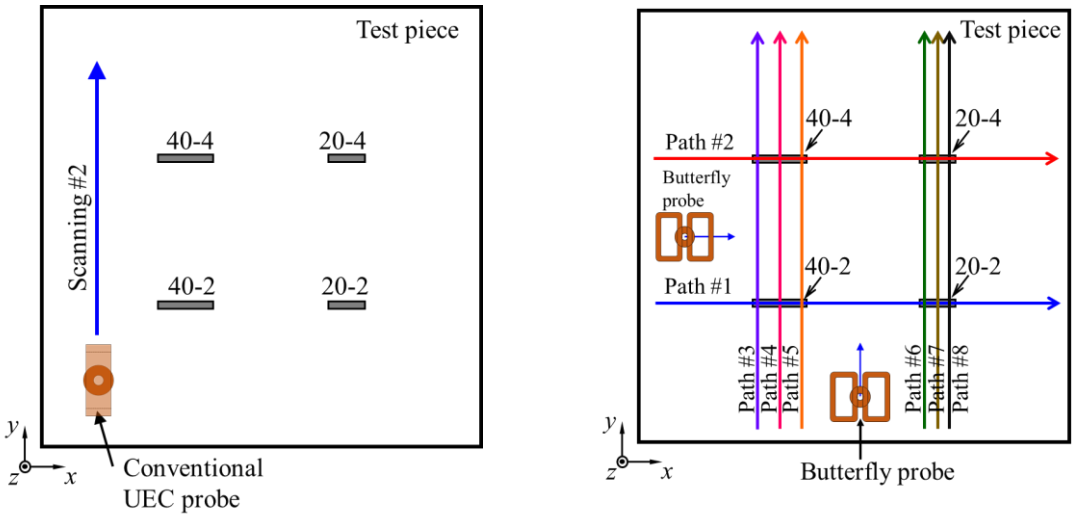

Figure 3.11 Scanning areas and paths on test piece: (a) scanning direction in the *x*-*y* area; the probe axis is perpendicular to the length of flaws, (b) scanning direction in the *x*-*y* area; the probe axis is parallel to the length of flaws test piece rotates 90˚, (c) scanning #2 for conventional UEC probe. (d) scanning paths direction.

In path scanning, measuring only one line follows the direction of each path.

3.4.1. Measurement results on scanning #1 and scanning #2

3.4.1.1. Testing using the Butterfly probe

The probe axis is perpendicular to the length of flaws

The results of butterfly probe testing with scans # 1 and # 2, as shown in Figure 3.11(a) are shown in Figures 3.12 and 3.13, respectively. In both, flaws detected clearly, and the measurement signal has a pair of peaks for each flaw. The distance between the two peaks represents the length of a flaw. The amplitude of the peak represents the depth of a flaw. When the probe passes through the middle of the defect length, the detector coil did not produce a significant signal because the EMFs on the sides of the detector is in a balanced condition.

To supply an excitation current of 6 mA, a voltage source is given at 6.5 Vpp. This

means that the probe is supplied with a power of approximately 14 mW.

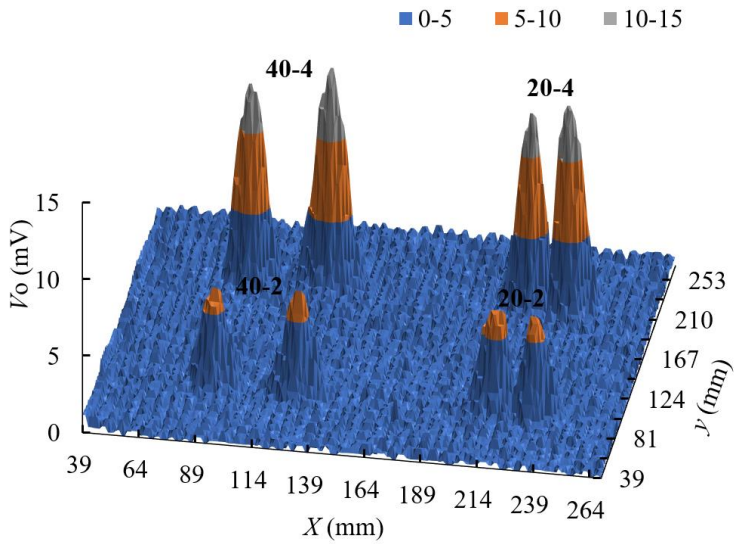

Figure 3.12 Measurement results of butterfly probe with scanning #1 in *x*-y area; The probe axis is perpendicular to the length of flaws. V_i=6.5 Vpp and I_i=6 mA.

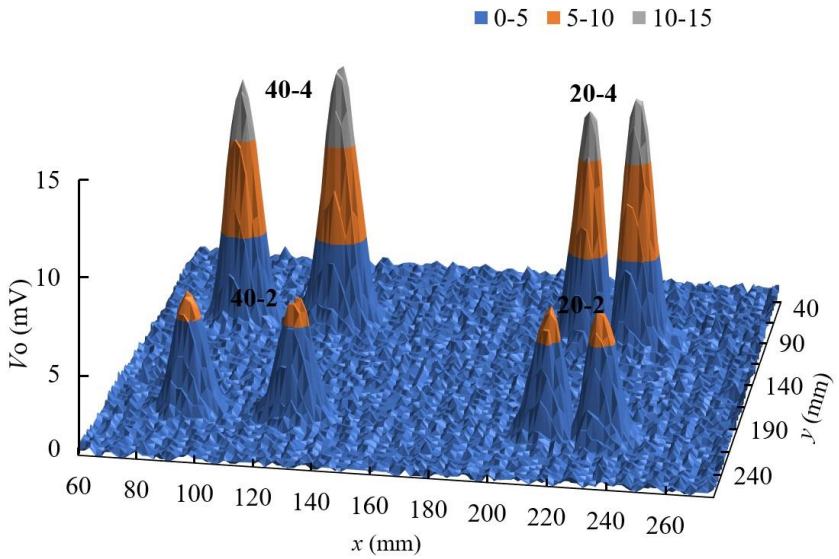

Figure 3.13 Measurement results of butterfly probe with scanning #2 in *x*-*y* area; The probe axis is perpendicular to the length of flaws. V_i=6.5 Vpp and I_i=6 mA.

Both results were relatively similar, where the flaw with the same depth has a similar amplitude, although the flaw length differs, 20 mm and 40 mm.

The probe axis is perpendicular to the length of flaws

The results of butterfly probe testing with scans # 1 and # 2, as shown in Figure 3.11(b) are shown in Figures 3.14 and 3.15, respectively. In both cases, flaws could not be detected at all on the entire surface. This situation occurs because the eddy current parallel to the length of the flaw does not cause significant distortion on eddy current flowing, so it does not affect the balanced coil condition of the detector, and hence no EMFs appears.

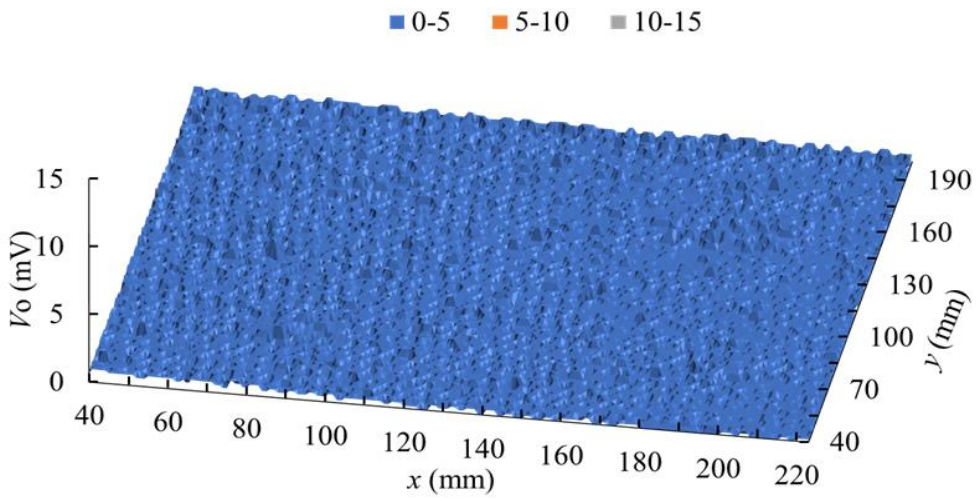

Figure 3.14 Measurement results of butterfly probe with scanning #1 in *x*-*y* area; Axis of probe parallel to the length of flaws. V_i=6.5 Vpp and I_i=6 mA.

From these results, for the implementation testing on the test piece, scanning must be done twice in a different direction 90° from the axis of the probe to ensure that the surface is clean of flaws.

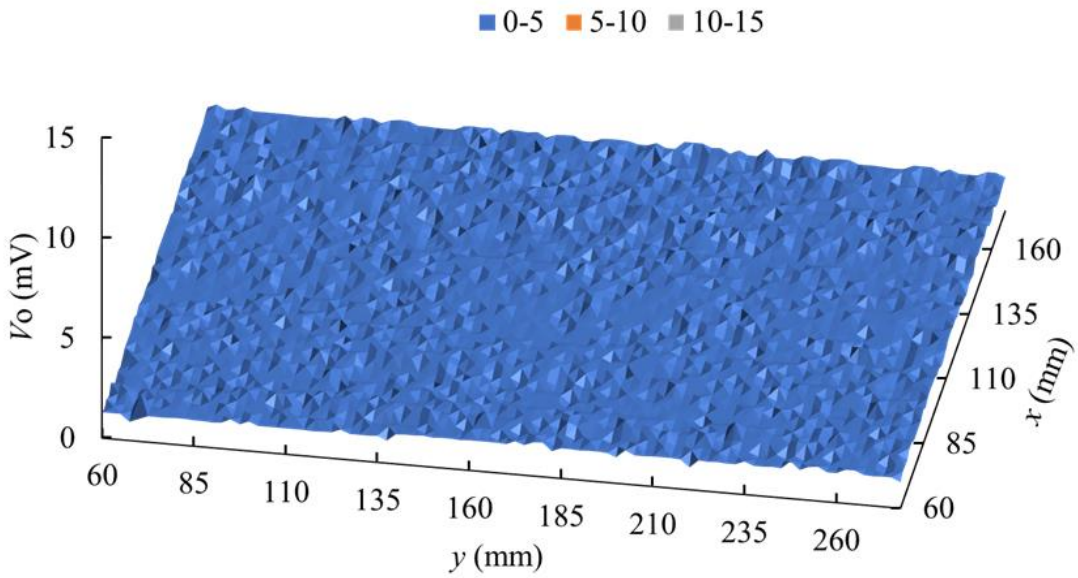

Figure 3.15 Measurement results of butterfly probe with scanning #2 in *x*-*y* area; Axis of probe parallel to the length of flaws. V_i=6.5 Vpp and I_i=6 mA.

3.4.1.2 Testing using the Conventional UEC probe

The result of conventional UEC probe testing with scanning # 2, as shown in Figure 3.11(c), is shown in Figure 3.16. The measurement result has similarities to the Butterfly probe with scanning #2 Figure 3.13. The amplitude peak and the distance between peaks are relatively similar. However, to supply 6 mA excitation current to the excitation coil, the source should be set at 20 Vpp or supplied with 42 mW of power. Accordingly, the Butterfly probe, which only requires 14 mW of power for generating the same excitation currents, has an advantage more efficient of approximately 66% for exciter power consumption.

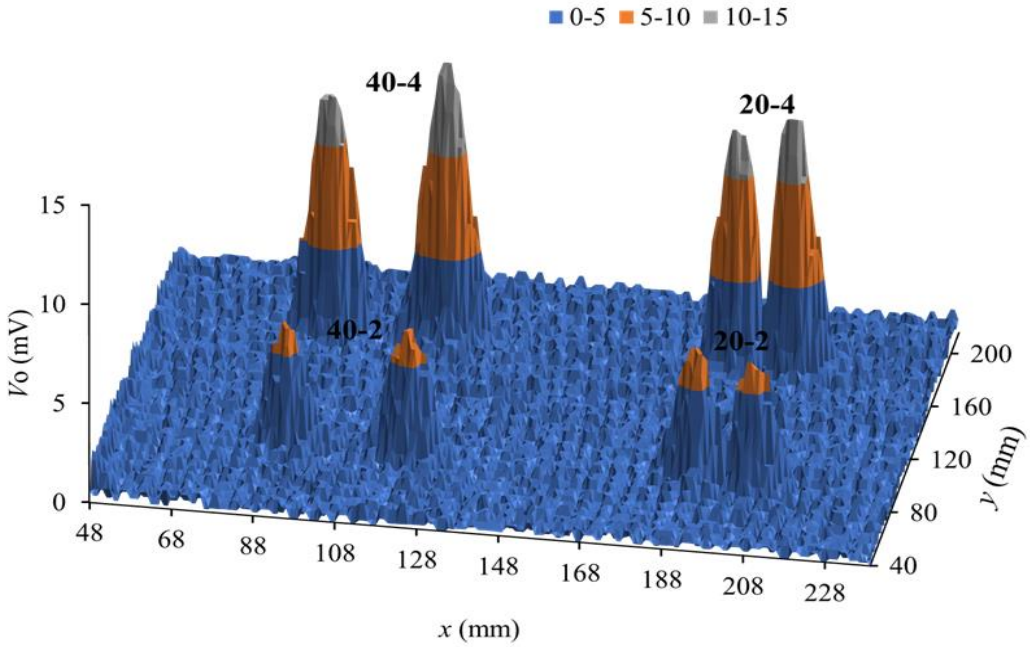

Figure 3.16 Measurement results of conventional UEC probe with scanning #2 in *x*-*y* area; The probe axis is perpendicular to the length of flaws. V_i=20 Vpp and I_i=6 mA.

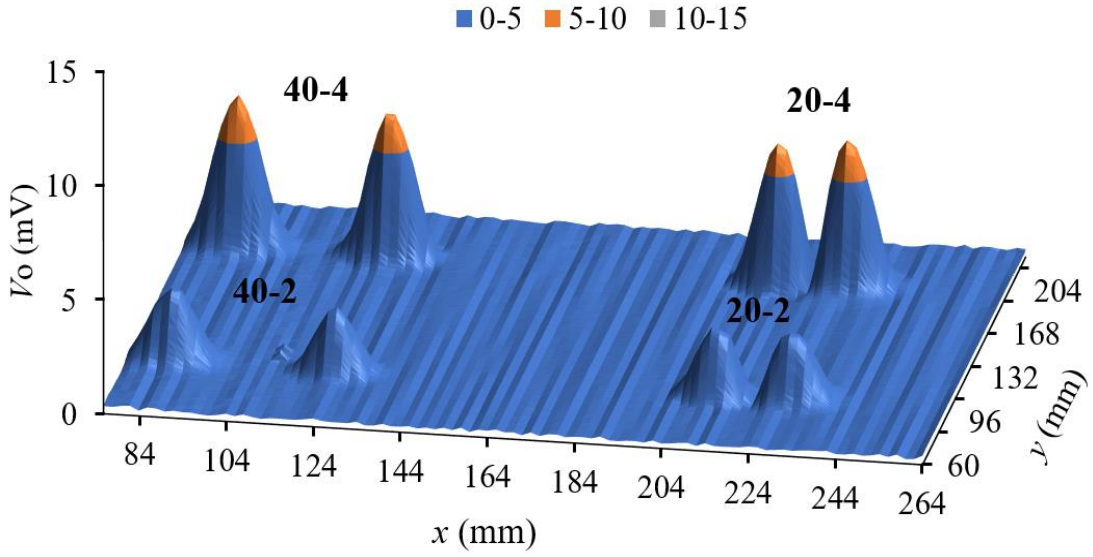

Figure 3.17 Measurement results of conventional UEC probe with scanning #2 in *x*-*y* area; The probe axis is perpendicular to the length of flaws. V_i=9.5 Vpp and I_i=4.2 mA.

When the excitation supply is made equal to around 14 mW, with an input voltage of 9.48 Vpp and an excitation current of 4.2 mA, the results obtained, as shown in Figure 6.17. The detection signal peaks are smaller by almost half of measurements with the butterfly probe.

In theory, efficiency occurs, can be explained by referring to the equivalent circuit of coil interactions to test pieces in Figure 2.3. Equation (2.12) determines the eddy current density I_e. We rewrite,

$$I_e = \frac{j\omega M_1 I}{R_e + jX_m + j\omega L_1} \tag{2.12}$$

Where $M_1 = kL_0$, so the equation becomes,

$$I_e = \frac{j\omega kL_0 I}{R_e + jX_m + j\omega L_1} \tag{3.7}$$

L_0 is a coil with pancake position, where all the coil surface is close to the surface of the test piece, and both interact with each other. In the tangential position, only a portion of the coil near the surface that is interacting. In this position, L_0 becomes smaller, we assume to be L_0/x, therefore,

$$M_1 = \frac{kL_0}{x} \tag{3.8}$$

Then the equation becomes,

$$I_{e\mathrm{T}} = \frac{j\omega \left(kL_0/x\right) I}{R_e + jX_m + j\omega L_1} \tag{3.9}$$

$I_{e\mathrm{T}}$ is eddy current density under tangential position. Hereafter, the equation is simplified to be,

$$I_{e\mathrm{T}} = \frac{j\omega kL_0 I}{x(R_e + jX_m + j\omega L_1)} \tag{3.10}$$

Equation (3.10) shows that the eddy current $I_{e\mathrm{T}}$ in the tangential position becomes smaller due to the ratio of $1/x$ of the coil surface that can interact with the surface of

the test piece.

3.4.2. Measurement results along paths #1 and #2 with scanning #1

Scanning using the Butterfly probe

Butterfly probe moves along paths #1 and #2, as shown in Figure 3.11(d). Scanning #1 results are shown in Figure 3.18 as a quantitative measurement of flaws. The peak voltages for 40-4 and 20-4 flaws are approximately 12 mV and for 40-2 and 20-2 flaws approximately 6 mV.

The length of the flaw is given by the distance between the two signal peaks, whereas the signal amplitude indicates the flaw depth. Hence, flaws with the same lengths, such as 40-4 and 40-2, or 20-4 and 20-2, the distance between two peaks of measured signals correspond to flaw length.

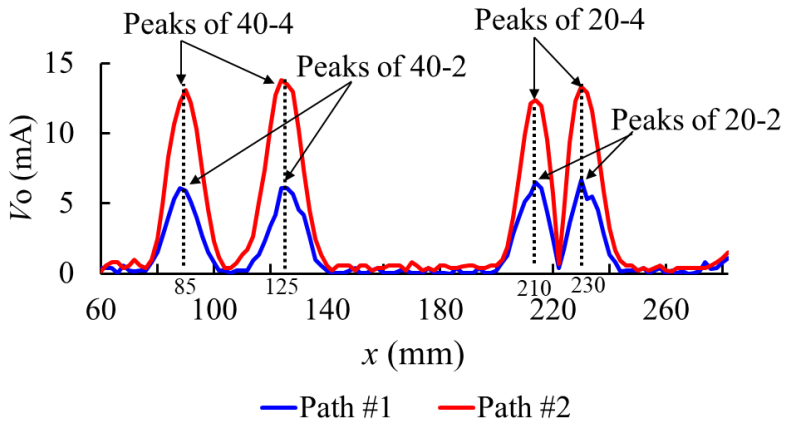

Figure 3.18 Measurement results of butterfly probe along paths #1 and #2. Excitation Supply is 14 mW; V_i=6.5 Vpp and I_i=6 mA.

The peaks of the signal for 40-4 are twice that of the signal for 40-2. Because the tendencies of the signals for 20-4 and 20-2 are same, the flaw depth can be quantitatively evaluated based on the amplitude of measured signals.

Scanning using the conventional UEC probe

To energize the conventional UEC probe, at a current supply maintained 6 mA, the supply voltage set to 20 Vpp, supplied with 42 mW of power. The scanning results in paths # 1 and # 2 are shown in Figure 3.19. The peak voltages for the 40-4 and 20-4 flaws is approximately 12 mV and for the 40-2 and 20-2 flaws is approximately 6 mV. These results show relatively the same as the scan performed with the Butterfly probe.

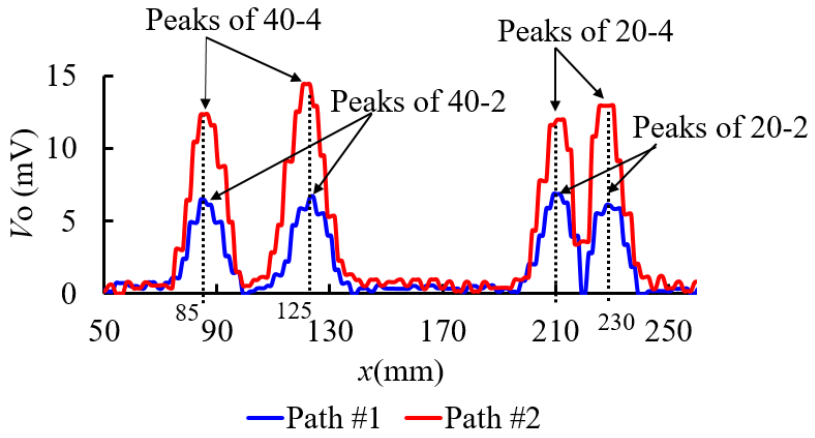

Figure 3.19 Measurement results of conventional UEC probe along paths #1 and #2. Excitation Supply is 42 mW; V_i=20 Vpp and I_i=6 mA.

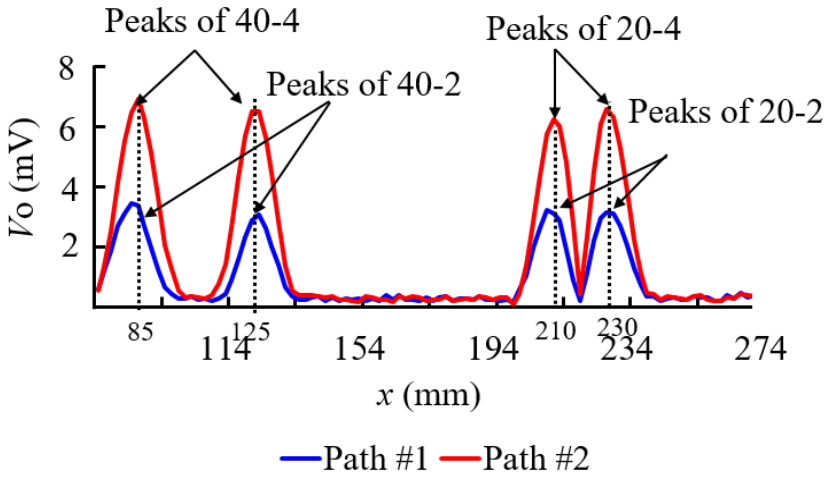

Figure 3.20 Measurement results of conventional UEC probe along paths #1 and #2. Excitation Supply is 14 mW; V_i=9.5 Vpp and I_i=4.2 mA.

However, when energizes for conventional UEC probes were made equal at around 14 mW, where the supply voltage was 9.5 Vpp, and the excitation current was 4.2 mA, the scanning results at paths # 1 and # 2 are shown in Figure 3.30. The peak voltage for the 40-4 and 20-4 flaws is smaller, approximately 7 mV, and for the 40-2 and 20-2 flaws approximately 3.5 mV. These results indicate that the peak of the signal is relatively smaller by almost half of the detection signal produced by the Butterfly probe. In other words, the detection signal of the butterfly probe is 1.7 times greater than the conventional UEC probe signal.

3.4.3. Measurement results along paths #3 until #8 with scanning #2

To observe the butterfly probe has self-differential and self-nulling characteristics, the probe moved along paths # 3– # 8 with scan # 2; the results are shown in Figure 3.18. When scanning in lines # 4 and # 7, no significant signal appears. This condition occurs because the detector coil is in a balanced condition and shows the characteristics of self-nulling and self-differential working, as shown in Figure 3.2 (b).

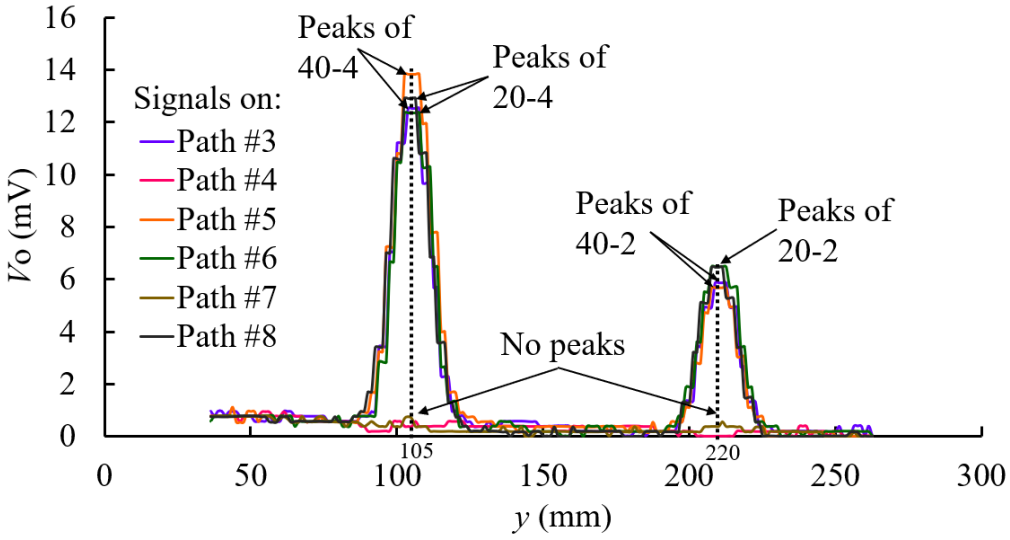

Figure 3.21 Measurement results of butterfly probe along paths #3 until #6.

Furthermore, the signals along paths #3, #5, #6 and #8 indicate two different peaks for two flaws. The first peak is approximately 12 mV, and the second is approximately 6 mV, which is half of the first signal amplitude. The ratio of V_o measurements is precisely the same as the flaw depth ratio.

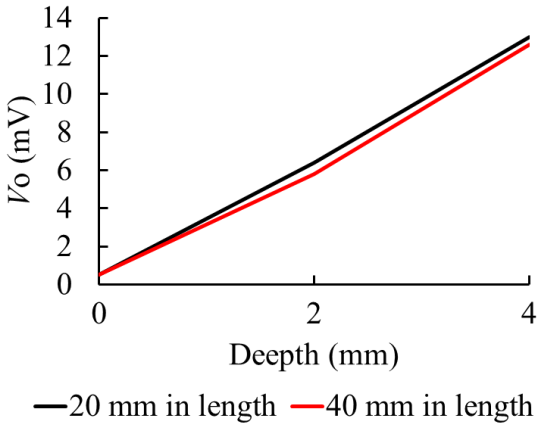

Figure 3.22 Effect of flaw length and depth on signal amplitude.

The results indicate that the probe can accurately evaluate flaws. The butterfly probe is also useful in evaluating flaw depth with scanning #2, which is for the angle of flaw; scanning #2 differs from scanning #1 by 90°.

The effect of flaw length and depth on signal amplitude shows in Figure 14. The amplitude is approximately the same as the flaw depth. This indicates that the length of the flaw does not have a significant influence on evaluating flaw depth.

From the results of scanning #1 and #2, there was no significant difference from the detection signals. Finally, an essential requirement for improving the quality of the butterfly probe measurement signal is on making excitation coil pairs. Each excitation coil must have the same specifications. Then, to get the best-balanced position, setting the detector coil must be located right in the middle of the axis of the pair of adjacent

excitation coils. These settings are to ensure the characteristics of self-differential and self-nulling.

3.5. Summary

The proposed one-directional Butterfly Probe has been used in experiments to detect various flaws on aluminum plates. The conclusions of the present study are as follows;

1. Implementation of the butterfly probe design to detect flaws on the aluminum plate was presented.
2. Analysis with finite element simulation, the butterfly probe succeeded in increasing the eddy current density by approximately 1.8 times that of the conventional UEC probe of the Hoshi probe model.
3. Testing on aluminum plates containing flaws, butterfly probes can detect flaws clearly; each defect is expressed by a signal that has a pair of peaks whose distance between the two peaks corresponds to the length of a flaw. Furthermore, the amplitude of the signal peak correlates with the flaw depth.
4. Experiments show that the Butterfly probe successfully increased the detection sensitivity up to 1.7 times compared to conventional UEC probes with a more efficient power consumption of approximately 66%.
5. The self-differential and self-nulling characteristics of the butterfly probe can be seen in the absence of a signal that appears significantly when the probe passes through the middle of the flaw length. This situation is due to the probe detection coil under balanced conditions. Meanwhile, the most significant signal is generated when the detection coil is right at the end of the flaw.

6. As long the axis of the butterfly probe is perpendicular to the length of the flaw, the probe can diagnose the flaw thoroughly by scanning one or scanning #2, which both direction different 90°.
7. Evaluation of measurements of flaw variations shows that the length of the flaw does not significantly affect the results of the size of the flaw depth. Accordingly, the butterfly probe can be considered in terms of reliable evaluation of flaw depth.
8. The precise setting of the detection coil position in the middle of the axis of the adjacent excitation coil pair determines the quality of the resulting measurement signal.

Chapter 4
4. Butterfly Probe with Rotating Uniform Eddy Current

4.1. Introduction

Eddy current testing using electromagnetic phenomena is a very useful method for detecting flaws such as cracks on the surface of a test piece and is widely used in the industry [27,51,55,56,57]. Eddy current probes have been used to enhance the signal/noise (S/N) ratio [58].

Two approaches are employed for the development of eddy current probes. The first involves the increase in the intensity of the generated eddy current by modifying the position and shape of the excitation coils. The second is to improve the electromotive force of the detection coil by modifying its position and shape; this improvement in the electromotive force is a function of the interaction zone, the nature of self-differential, and self-nulling [8,59,60,61].

To achieve a high S/N ratio from the signal, a UEC probe is used [10,19]. A UEC probe is a specially designed probe such that the configuration of the excitation coil provides UEC distribution, and the detection coils are characterized by self-differential and self-nulling features [51].

A Hoshi probe, as a fundamental UEC probe, was invented by Hoshikawa. It

consists of a large tangential rectangular excitation coil and a small pancake circular detection coil whose position is in the backside surface of the middle of the excitation coil. A Hoshi probe was designed to detect flaws such as flaws on the weld zone having uneven surface a nonmagnetic material [10,43]. By improving the detectability of the flaw based on further studies by Hoshikawa, a cross probe and plus probe of the UEC probe were invented. The cross probe consists of a large tangential rectangular excitation coil and a large tangential rectangular detection coil, while the plus probe consists of a large tangential rectangular excitation coil and two tangential rectangular detection coils [3,26,28]. Another type, a developed tangential eddy current array probe, can provide a clear measurement signal of surface flaws despite changes in lift-off and permeability [62].

As one of the UEC probe types, UEC probe with a giant magnetoresistance (GMR) detector (that is, in conjunction with a magnetic sensor) was studied. The probe consists of one tangential rectangular excitation coil and a GMR detector. The probe can work at frequencies below 1 kHz, and thereby, can detect deeper flaws from the surface of the test piece [31,32,63]. A similar type, using a tunnel magnetoresistance sensor, with a rotating UEC orientation, was able to detect flaws in carbon fiber reinforced polymers with variation in orientation and length of the flaws [64].

The recent probe design that uses the UEC principle is a differential planar eddy current probe, was called the IOnic probe. The probe consists of one tangential rectangular excitation coil and two pancake semicircular planar coils as the detector and is capable of detecting fine flaws. However, the production of the probe requires high precision as the symmetrical planar spiral detectors must be identical on both sides [36,40,46].

In the UEC probe, the excitation coils are tangentially oriented to generate UEC

distribution. However, this orientation provides a weak induction on the test piece, resulting in low amplitude of UEC as well. Recently, a new UEC probe consisting of a pair of rectangular excitation coils and a detector coil that are pancake-oriented was developed by our research group and was called a one-directional butterfly probe by the authors [46,53]. This probe has a large electromagnetic field induction on the test piece, and thereby has the advantage of a large S/N ratio. However, the butterfly probe uses a unidirectional UEC, and it has the disadvantage of not being able to detect a flaw whose direction is parallel to the flow of UEC.

Therefore, to overcome this disadvantage, the one-directional butterfly probe was improved. In this study, a UEC probe consisting of two pairs of rectangular pancake excitation coils arranged in two layers and a circular pancake detection coil has been proposed. The configuration of the probe was designed so as to generate a rotating UEC that is able to detect flaws in all directions. This was called the butterfly probe with rotating uniform eddy current (BPRUEC) by authors. The UEC distribution by a BPRUEC was analyzed via finite element simulation. Furthermore, experiments were carried out to examine the detectability of flaws in all directions on the surface of an aluminum plate.

4.2. Materials and Methods

4.2.1. Structure Coils of BPRUEC

A one-direction butterfly probe proposed in a previous study [21] was modified into a BPRUEC. The structure of the BPRUEC is shown in Figure 4.1. It consists of two pairs of rectangular excitation coils arranged in two layers whose longitudinal axes are perpendicular to each other. A circular detection coil is present at the bottom middle of the probe.

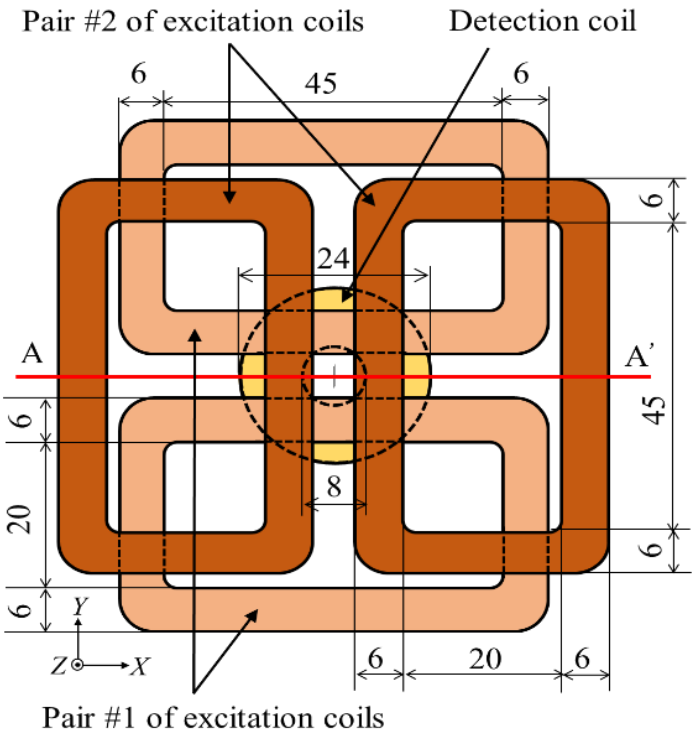

(a)

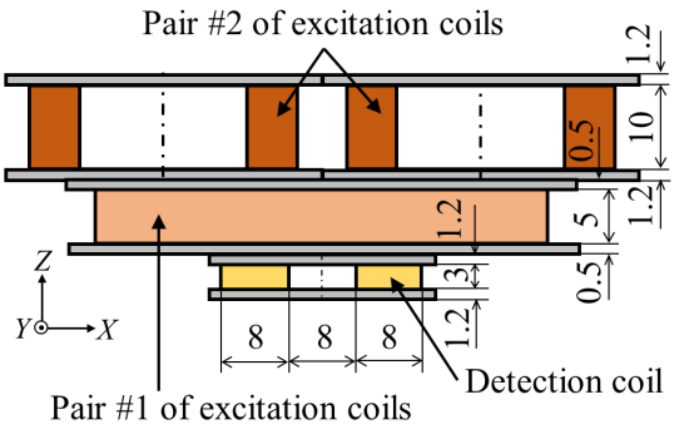

(b)

Figure 4.1 The structure of the coils in a BPRUEC, all dimensions in mm, (a) top view (b) section view of A-A'.

The number of turns of each excitation coil of pair #1 of excitation coils was 500, the total number of turns being 1000. The number of turns of each excitation coil of pair #2 of excitation coils was 1000; thus, the total number of turns was 2000. The purpose of

a larger number of turns of coils for pair #2 was to induce the same induction strength to the test pieces as pair #1, considering that the former has a larger lift-off value (11.5 mm). The number of turns of the detection coil was 330 turns.

Since the two pairs of the excitation coils were orthogonally installed, it is assumed that UEC_1 generated from pair #1 of the excitation coils flows in *y* direction, while UEC_2 generated from pair #2 of the excitation coils flows in *x* direction. UEC_1 and UEC_2 are, respectively, the UECs that are generated by pair #1 and #2 of excitation coils, using two excitation currents for which the phase difference is 90°. The rotating UEC is the resultant UEC (*RUEC*) of the UECs generated by pair #1 and pair #2 of the excitation coils, as given by the following equations:

$$UEC_1 = A\ sin\left({}^{2\pi t}/_{T}\right) \tag{4.1}$$

$$UEC_2 = A\ sin\left({}^{2\pi t}/_{T}\right) + {}^{\pi}/_{2} \tag{4.2}$$

$$RUEC = \sqrt{(UEC_1)^2 + (UEC_2)^2} \tag{4.3}$$

$$\varphi_R = \tan^{-1}\left(\frac{UEC_1}{UEC_2}\right) \tag{4.4}$$

where *T* is the period of the excitation current, *A* is the amplitude of the UECs, and φ_R is the *RUEC* direction on the surface of the test piece. When two excitation currents are flowing in the same period, *RUEC* is rotated in all directions with constant amplitude. Figure 4.2 shows the rotating UEC distribution when using the BPRUEC.

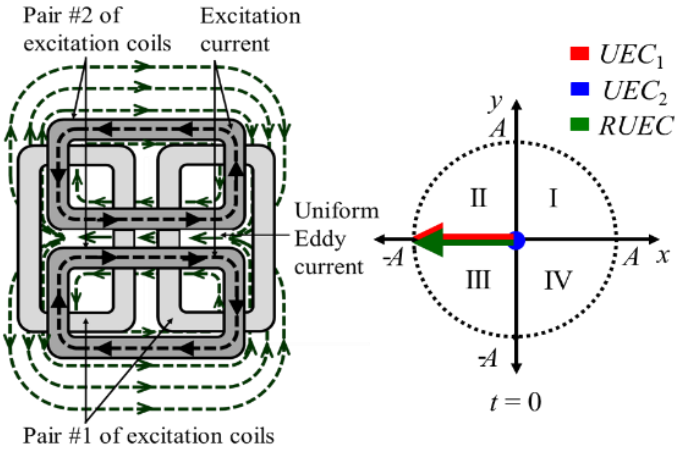
Pair #2 of excitation coils
Excitation current
Uniform Eddy current
Pair #1 of excitation coils
UEC_1
UEC_2
$RUEC$
y
A
II
I
-A
A
x
III
IV
-A
$t = 0$

(a)

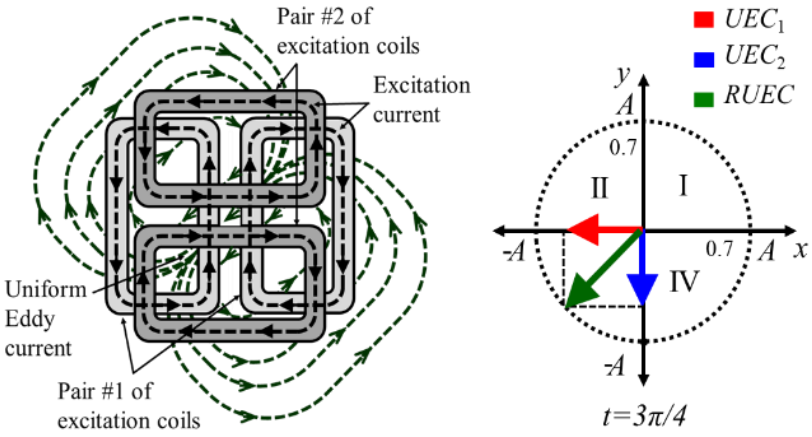
Pair #2 of excitation coils
Excitation current
Uniform Eddy current
Pair #1 of excitation coils
UEC_1
UEC_2
$RUEC$
y
A
0.7
II
I
-A
0.7
A
x
IV
-A
$t=3\pi/4$

(b)

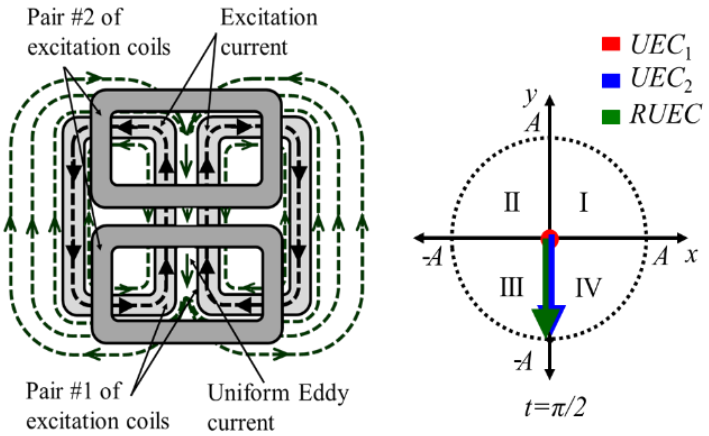
Pair #2 of excitation coils
Excitation current
Pair #1 of excitation coils
Uniform Eddy current
UEC_1
UEC_2
$RUEC$
y
A
II
I
-A
A
x
III
IV
-A
$t=\pi/2$

(c)

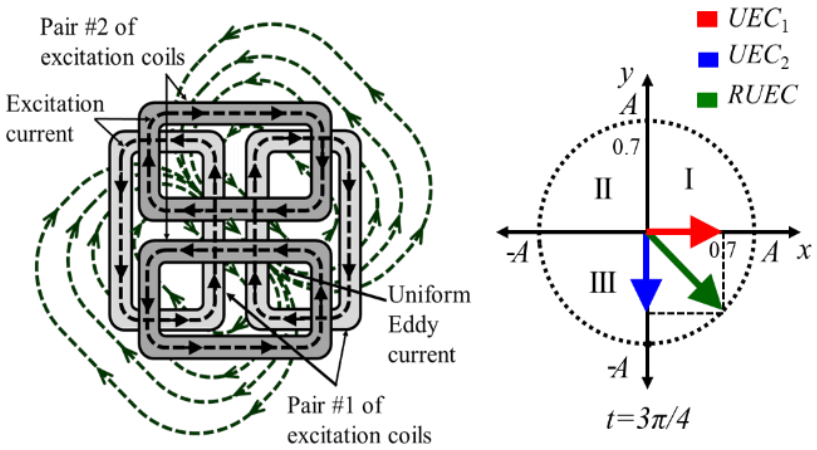

(d)

Figure 4.2 The UEC distribution with the BPRUEC (a) $t = 0$, (b) $t = \pi/4$, (c) $t = \pi/2$, and (d) $t = 3\pi/4$.

The principles of the electromotive force of pancake circular detection coil with flaws and without flaws are the same as that of a one-directional UEC probe. There are two conditions of the detection coil in the butterfly probe: balanced and unbalanced. These conditions are determined by the response of the interaction zone of the detection coil against the UEC, as shown by the red dotted line in Figure 4.3.

Under the balanced condition, ε_1 and ε_2 of the electromotive forces of the detection coil are of the same amplitude, but opposite in polarities, as shown in Figure 4.3(a). As a result, they cancel each other out. This phenomenon is called self-nulling, where the detection coil output is zero. The output is also zero when the probe is positioned in the middle of a flaw, as shown in Figure 4.3(b); this is because the eddy currents have the same disturbance on both the sides of the detection coil.

The model in which the edge of a flaw is located under the detection coil is shown in Figure 4.3(c). Because the disturbance caused by the flaw caused ε_1 and ε_2 of the detection coil to have unequal amplitudes, an output is generated.

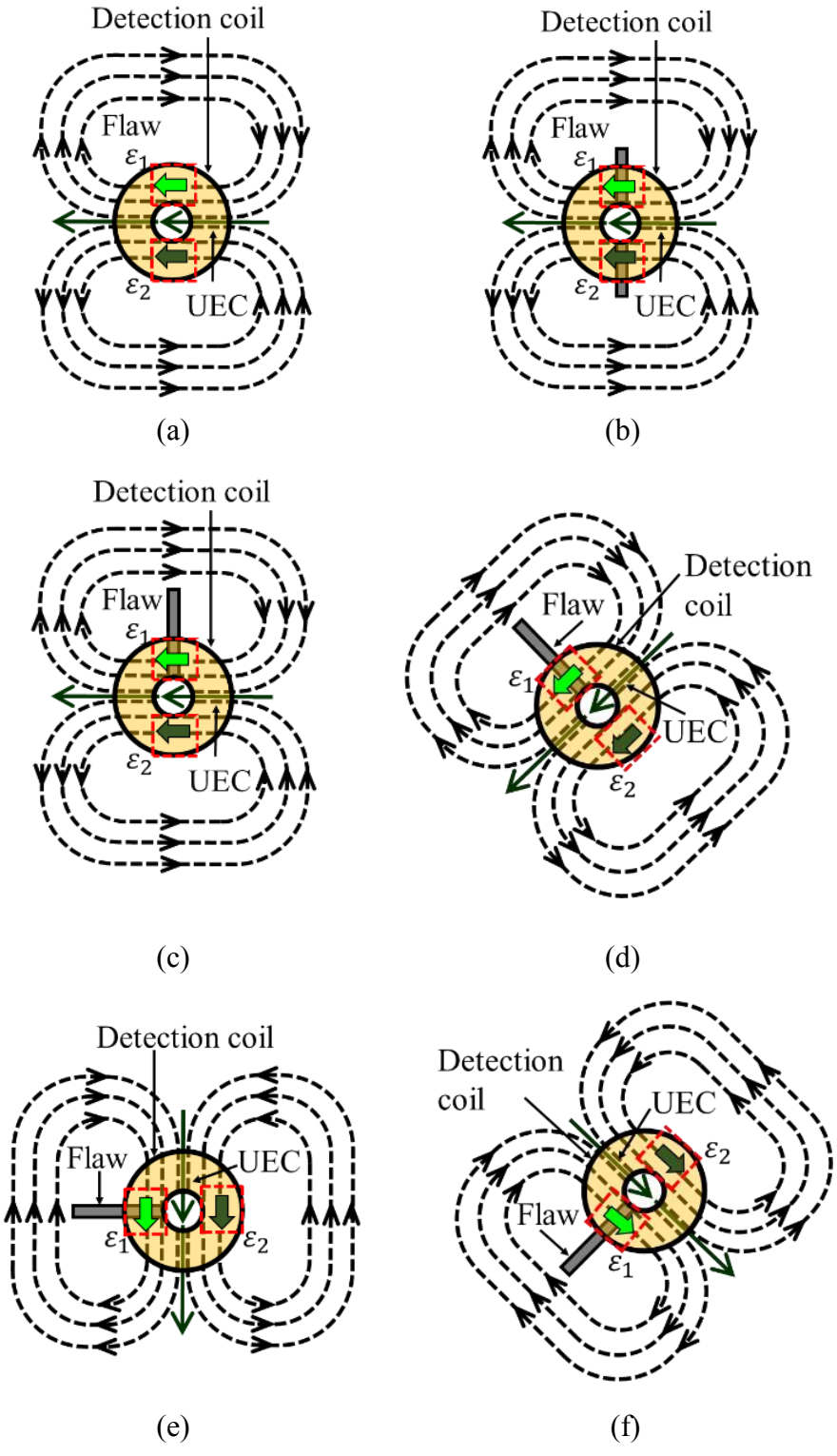

Figure 4.3 The rotating UEC (RUEC) distribution patterns of the BPRUEC based on the excitation signal cycle. (a) RUEC at 0 position, (b) RUEC at π/2 position, (c) RUEC at π/4 position, and (d) RUEC on 3π/4 position.

When there is a flaw on the surface of the test piece, the rotating UEC has a position perpendicular to that of the flaw, as shown in Figure 3(c), (d). In this position, the signal of the detection coil picks up the disturbance due to the flaw, which provides a maximum signal during the measurement.

Furthermore, the self-nulling characteristic of the detector coil maintains even under the rotating UEC distribution. Finally, to ensure high accuracy of the BPRUEC, the resultant UEC generated from pairs #1 and #2 of the excitation coils should have the same amplitude in all directions. Moreover, the excitation coils and the detector coil must have a self-nulling characteristic.

4.2.2. Numerical Calculations

The distribution of UEC on the surface of the test piece was analyzed with a time-harmonic analysis. In the analysis, with Magnet 7 version 7.4.1 from Mentor Graphics Corporation located in Wilsonville, Oregon USA, which used the current vector potential (T), the magnetic scalar potential (Ω) method was used. In conducting medium, the basic equations of the method are expressed by using Faraday's law and Ampere's law. Constitutive relation has described in equations (3.1) to (3.6), on previous chapter.

The element of the mesh was modeled as a linear superposition of polynomial basis function for high accuracy. The total number of meshes was 947,420. The analysis was carried out with the meshes of the BPRUEC and the area under the probe as small a size as possible within the performance of a personal computer.

Figure 4.4 shows the analytical model set up of the BPRUEC. The size and configuration of the rotating UEC probe were the same as those shown in Figure 4.1. In the analytical model, an aluminum plate test piece was modeled with dimensions of 120 mm in width, 120 mm in length, and 10 mm in thickness. Table 4.1 shows the

electromagnetic parameters used in the analysis.

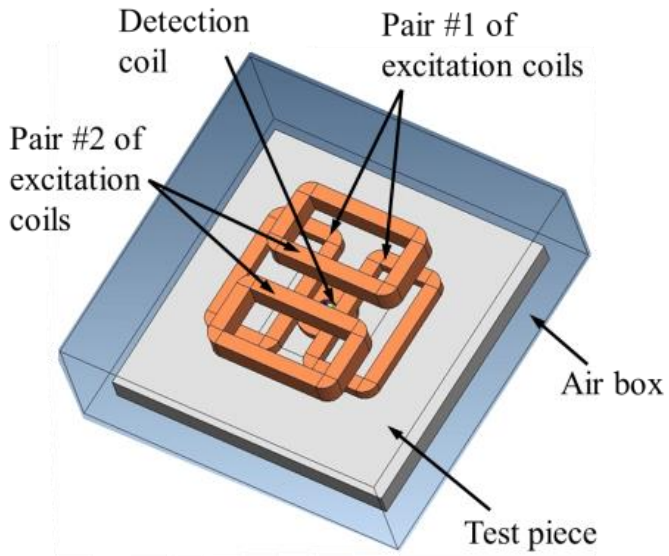

Figure 4.4 The analytical model set up for the BPRUEC.

Table 4.1 Electromagnetic parameters used in analysis.

Parameters	Copper Wire of Coil	Aluminum Test Piece
Electrical conductivity σ	57.7 MS/m	35 MS/m
Relative permeability μ	1	1

Pair #1 and #2 of the excitation coils were supplied with a 6.5 mA and 9.5 mA current, respectively, at a frequency of 10 kHz. The phase difference of the excitation currents between pair #1 of excitation coils was 90°.

Figure 4.5 shows the arrow plot of the UEC distribution on the surface of the test piece with the BPRUEC. When the phases of excitation currents were 0 and 90°, respectively, the UEC from pair #2 of excitation coils was at a maximum, while that from pair #1 was zero. As a result, the resultant UEC was formed in y direction, as shown in Figure 4.5(a). When the phases of excitation currents were 45°and 135°, respectively,

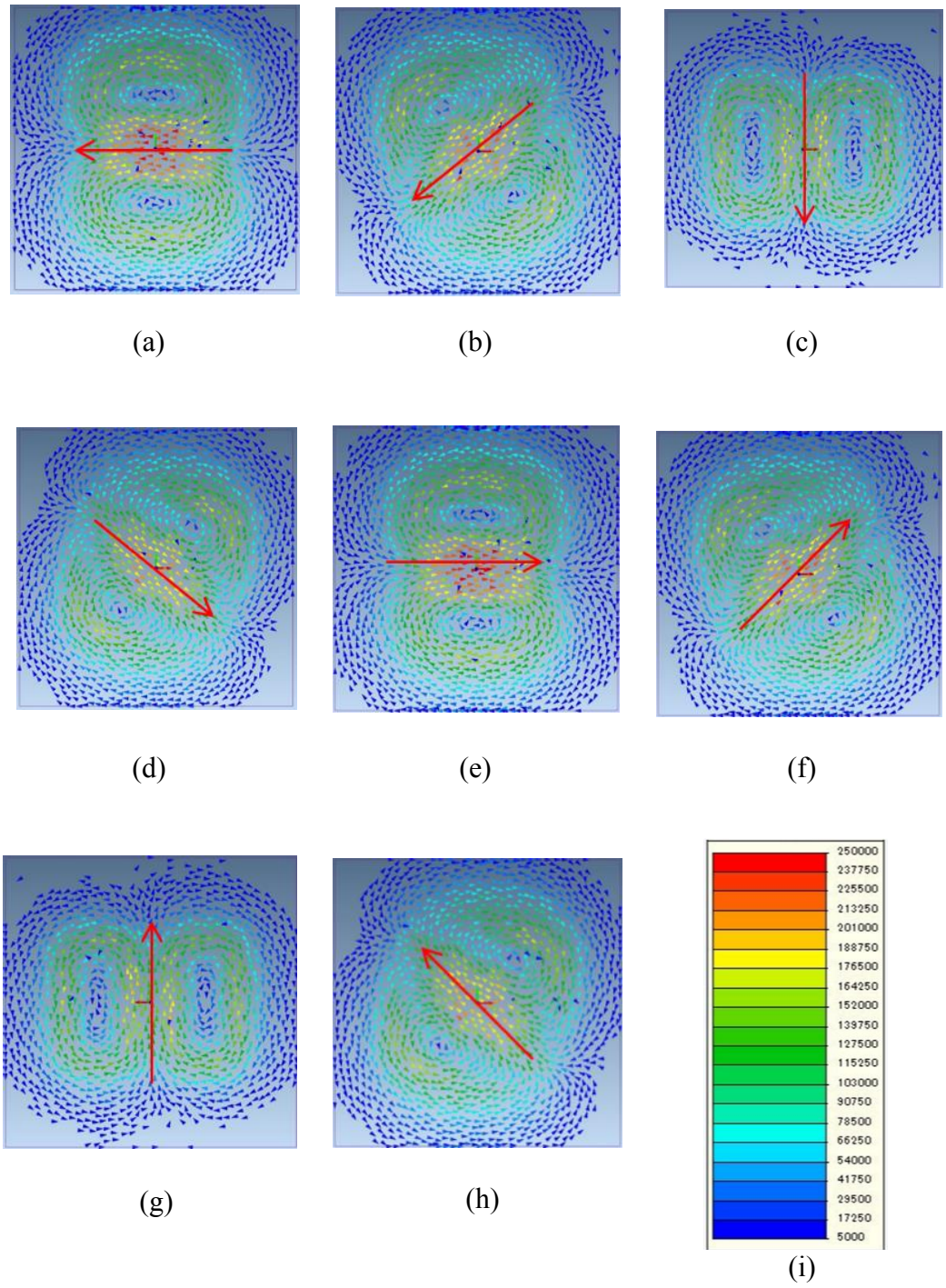

Figure 4.5 Arrow plot of the UEC distribution on the surface of the test piece with the BPRUEC. (a) $t = 0$, (b) $t = \pi/4$, (c) $t = \pi/2$, (d) $t = 3\pi/4$, (e) $t = \pi$, (f) $t = 5\pi/4$, (g) $t = 3\pi/2$, (h) $t = 7\pi/4$, and (i) Density of J.

the UEC from pair #1 and #2 of the excitation coils was of the same amplitude. Thus, the resultant UEC was formed at 135° as shown in Figure 4.5(b). When the phases of

excitation currents were 90° and 135°, respectively, the UEC from pair #1 of excitation coils was at a maximum, while that from pair #2 was zero. Therefore, the resultant UEC was formed in *y* direction, as shown in Figure 5(c).

Similarly, as shown in Figure 4.5(a)–(h), the distribution of UEC with the BPRUEC was in a counterclockwise direction. The intensity of the rotating UEC in the area under the middle of the probe was almost the same although the intensity of the UEC at 90°and 270° was a little lower.

4.3. Experimental Setup

Experimental set-up for testing the BPRUEC shown in Figure 4.6.

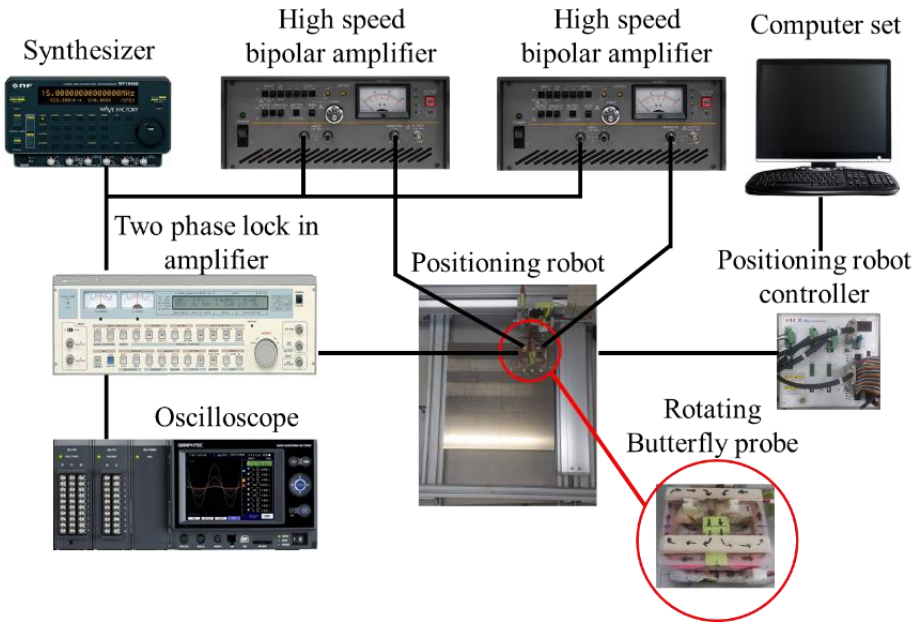

Figure 4.6 Experimental set-up for the BPRUEC testing.

Similar with previous experiment, the test plate was used aluminium plate 5052. On the surface, there are four artificial flaws whose sizes are listed in Table 3.3, and their positions are shown in Figure 3.8. Two excitation currents of sine wave with 10 kHz were

generated using a synthesizer. Two excitation currents, with a phase difference of 90°, were then amplified to 6.5 mA and 9.5 mA for pair #1 and #2 of the excitation coils, respectively, using high speed bipolar amplifiers. The signal of the detection coil was analyzed via a two-phase lock in the amplifier to obtain the amplitude and phase of the signal. The acquired data were stored using a digital oscilloscope having a frequency of 4 Hz.

The BPRUEC was moved by a positioning robot to scan the surface of the test piece. The robot's speed was set to 10 mm/s and the scanning interval was 2.5 mm for both the *x* and *y* directions. The distance between the probe and the surface of the test piece was approximately 1.2 mm.

4.3.1. Specification of Probe Coils

The specifications of the coils are summarized in Table 4.2.

Table 4.2 Specifications of coils of the BPRUEC.

Component		**Specification**	
Rotating butterfly probe	Pair #1 excitation coils	Wire diameter	0.2 mm
		Turns	2×500
		Resistance	42 Ω
		Inductance	157 mH
		Impedance	108 Ω
	Pair #2 excitation coils	Wire diameter	0.2 mm
		Turns	2×1,000
		Resistance	179 Ω
		Inductance	204 mH
		Impedance	1.27 kΩ
	Detection coil	Wire diameter	0.2 mm
		Turns	330
		Resistance	9.2 Ω
		Inductance	1.33 mH
		Impedance	12.44 Ω

4.3.2. Scanning Direction for BPRUEC

The BPRUEC has four scanning directions, as shown in Figure. 4.8. In scanning #1 and 2, to test the dominance of coil pairs on layer 1 to detect flaws. Then in scanning 3 and 4, to test the dominance of coil pairs on layer 2 to detect flaws.

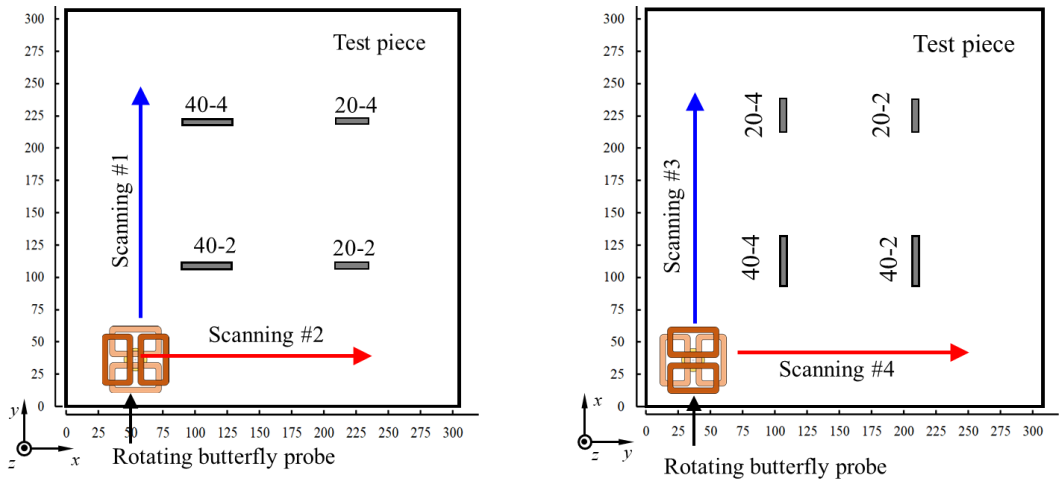

(a) (b)

Figure 4.7 Scanning position of the BPRUEC: (a) Scanning #1 and #2; (b) Scanning #3 and #4.

4.4. Results and Discussion

Figure 4.9 shows the scanning direction of the BPRUEC on testing. There are four patterns of scanning, as shown in Figure 4.9(a) and (b). Scanning #1 was for the BPRUEC moving along the *y* axis (blue line); it was repeated by shifting it in the *x* axis direction (red line). In scanning #2, the BPRUEC moved along the *x* axis (red line), and then was shifted in the *y* axis direction (blue line).

In scanning #3 and #4, the position of the test piece was rotated by 90° from its position during scanning #1 and #2. Scanning #3 involved the moving of the BPRUEC along the *y* axis (blue line), followed by shifting in the *x* axis direction (red line). In scanning #4, the probe moved along the *x* axis (red line), and then shifted in the *y* axis

direction (blue line). In scanning #1 and #2, the flaws were parallel to the *x* axis, and the axis of pair #2 of the excitation coils was perpendicular to the flaw lengths. In scanning #3 and #4, the flaws were parallel to the *y* axis, and the axis of pair #1 of the excitation coils was perpendicular to the flaw lengths. These scanning paths allow further discussion regarding the orientation of the flaws and the scanning paths.

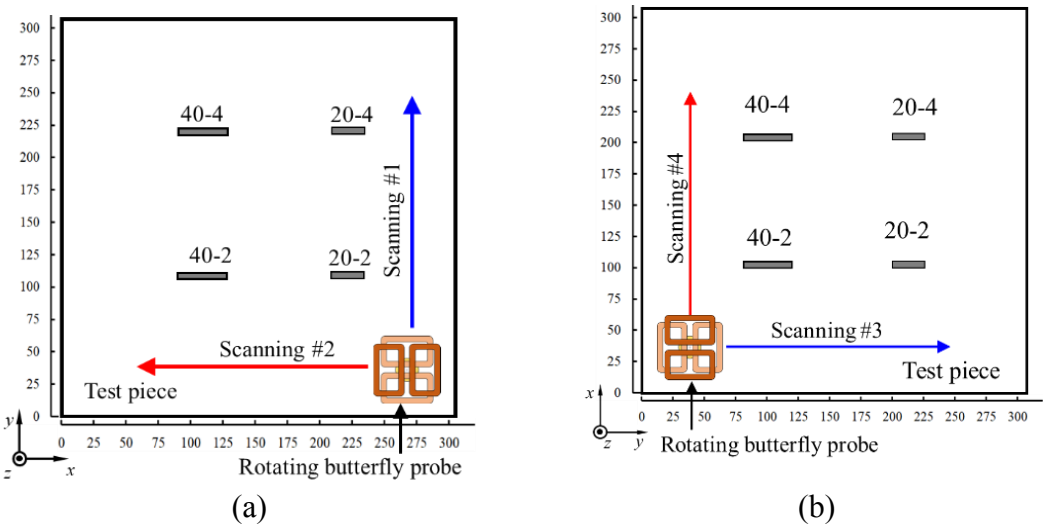

(a) (b)

Figure 4.8 Scanning direction of the BPRUEC. (a) The flaws are parallel to the *x* axis. The axis of pair #2 of the excitation coils is perpendicular to the flaw lengths. (b) The flaws are parallel to the *y* axis. The axis of pair #1 of the excitation coils was perpendicular to the flaw lengths.

The measurement results from scanning #1 to scanning #4 are shown in Figure 4.10. In general, the measurement results clearly distinguish the signals from flaws, which is indicated by the presence of two peaks of amplitudes for each flaw. However, there were significant differences in the amplitude and peak patterns of the amplitude between the results of scanning #1 and #2 compared with the results of scanning #3 and #4. The repeatability of measured results with the BPRUEC was investigated. As a result, similar results with a similar amplitude and distribution were obtained.

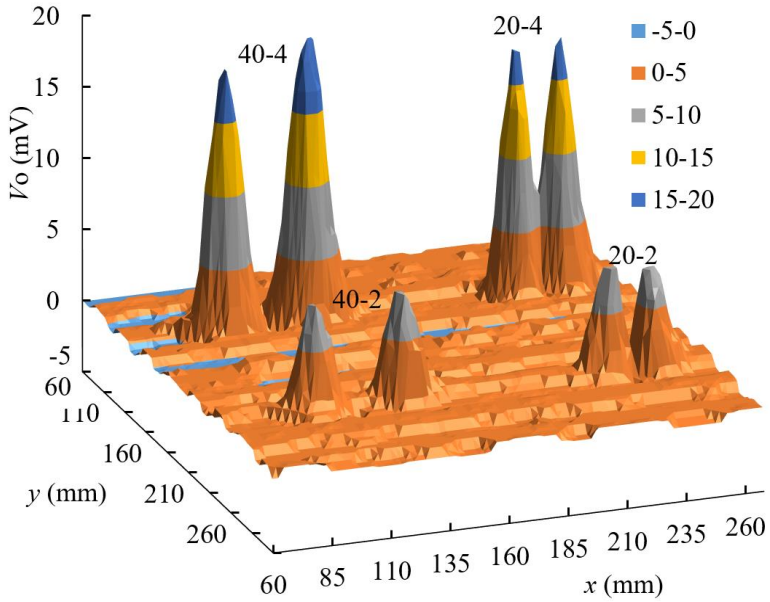
20
15
10
5
0
-5
Vo (mV)
40-4
20-4
40-2
20-2
-5-0
0-5
5-10
10-15
15-20
60
110
160
210
260
y (mm)
60
85
110
135
160
185
210
235
260
x (mm)

(a)

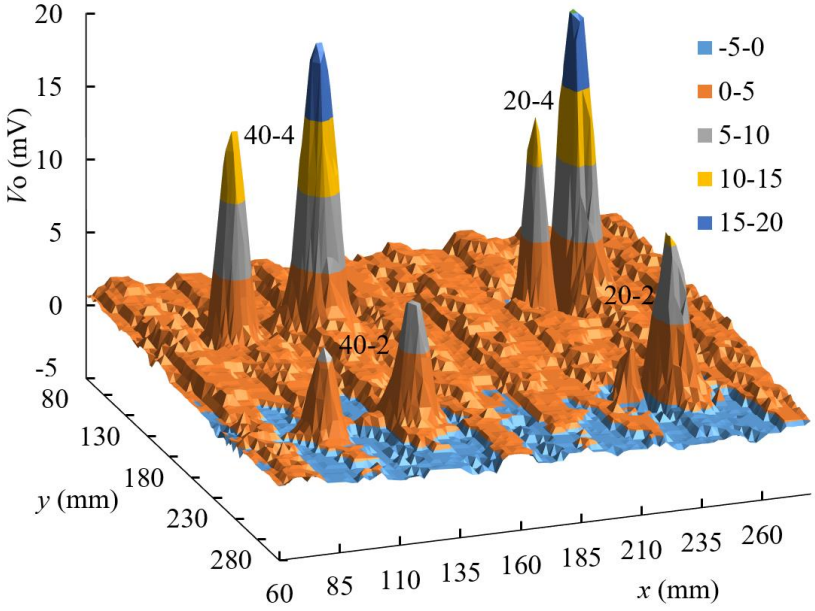
20
15
10
5
0
-5
Vo (mV)
40-4
20-4
40-2
20-2
-5-0
0-5
5-10
10-15
15-20
80
130
180
230
280
y (mm)
60
85
110
135
160
185
210
235
260
x (mm)

(b)

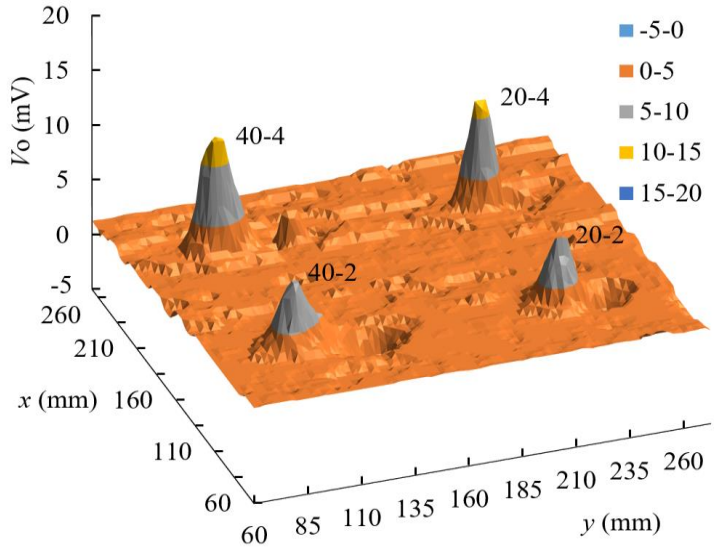

(c)

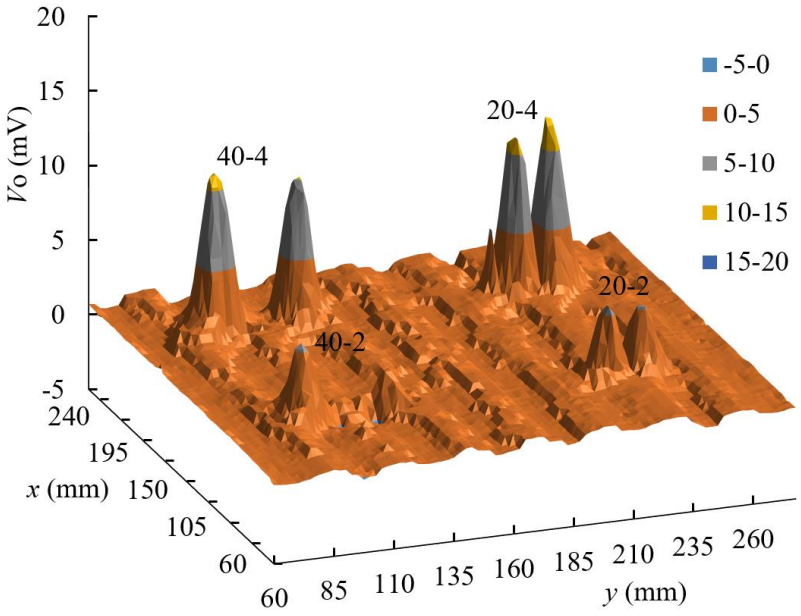

(d)

Figure 4.9 Measurement results (a) scanning #1, (b) scanning #2, (c) scanning #3, and (d) scanning #4.

4.4.1. Detection of flaws whose length is parallel to the *x* axis

In Figure 4.10(a), the two peaks of the signal on the edge of the flaw were relatively similar. The signals of 40-4 and 20-4 were approximately 18 mV, and the signals

of 40-2 and 20-2 were nearly 8 mV. The amplitude of the signal of flaw depth of 4 mm was twice as large as that of the flaw depth of 2 mm. Moreover, the distance between the peaks of the signal of each flaw corresponded to the flaw length itself.

Figure 4.10(b) shows the measurement result of scanning # 2. The signals were clear, although the two peaks of the signal from each flaw were not the same. The amplitude of peak at one end of a flaw, which was first scanned by the probe, was larger than that at another end of the flaw that was scanned subsequently.

4.4.2. Detection of flaws whose length is parallel to the *y* axis

The measurement results of scanning #3 are shown in Figure 4.10(c). All detection signals differed from the other measurement results, signifying that the signal did not have two peaks. However, the amplitude of the peak of the signal size was relatively similar to that in scanning #4.

Figure 4.10(d) shows the measurement result of scanning #4. Three flaws, 40-4, 20-4, and 20-2, were clearly detected with two signal peaks. The amplitude of the peaks of flaws 40-4 and 20-4 were approximately 11 mV, while the amplitude of the peaks of flaws 20-2 measure approximately 5.5 mV. However, the amplitude of the larger peak for the 40-2 flaw was approximately 5.5 mV, while the amplitude of another peak was almost half (approximately 3 mV).

4.5. Discussion

Based on the measurement results, two issues from experimental findings were analyzed. The first issue was that the peak amplitude of scanning #1 and #2 was approximately 1.5 times higher than those of scanning #3 and #4. This was caused by the influence of induction strength that dominates from pair #1 and #2 of excitation coils in

the measurement. By considering the structure of the butterfly probe and the mounting condition of the probe to the positioning robot, the predominant factor affecting the amplitude of the peak of the signal was whether the axis of the excitation coils was perpendicular to the flaw length or not. In scanning #1 and #2, the axis of pair #2 of the excitation coils was perpendicular to the flaw length, while, in scanning #3 and #4, the axis of pair #1 of the excitation coils was perpendicular. Moreover, the number of turns of pair #2 of the excitation coils was twice than that of pair #1. In addition, the excitation current was also 1.5 times higher for pair #2 than that for pair #1. These differences between pair #1 and pair #2 of the excitation coils were intended to balance the strength of the induction to generate the rotating UEC with the same amplitude in all directions by considering the different lift off values, which were 11.5 mm for pair #2 and 4.2 mm for pair #1 of the excitation coils. However, the difference was insufficient to generate the rotating UEC with same amplitude in all directions. The induction of pair #2 of the excitation coil was larger than that of pair #1 of the excitation coils, so that the amplitude of the peak of the signal dominated by pair #2 was larger than that dominated by pair #1 of the excitation coils.

The second issue was that the amplitude of two peaks of the detection signal on the edge of each flaw were not relatively similar. This issue was evident from the results of scanning #2 and scanning #3. In these cases, the rotating probe moved toward the edge of the flaw and parallel to the flaw length; the UEC was of relatively high density, as it was compressed owing to the flaw, so that the signal of the electromotive force generated from the detection coil increased, as shown Figure 4.11(a). As the rotating probe moved away from the edge of the flaw, UEC at the area was relatively uncompressed, and the signal of the electromotive force generated from the detection coil decreased, described in Figure 4.11(b). Meanwhile, in scanning #1 and #4, as shown Figure 4.11(c), the

BPRUEC was moving toward the edge of the flaw and perpendicular to the flaw length. In these cases, UEC distributions on the edge of the flaw were almost same on both the edges of the flaw; as a result, the same amplitudes of the peaks of the signals were observed.

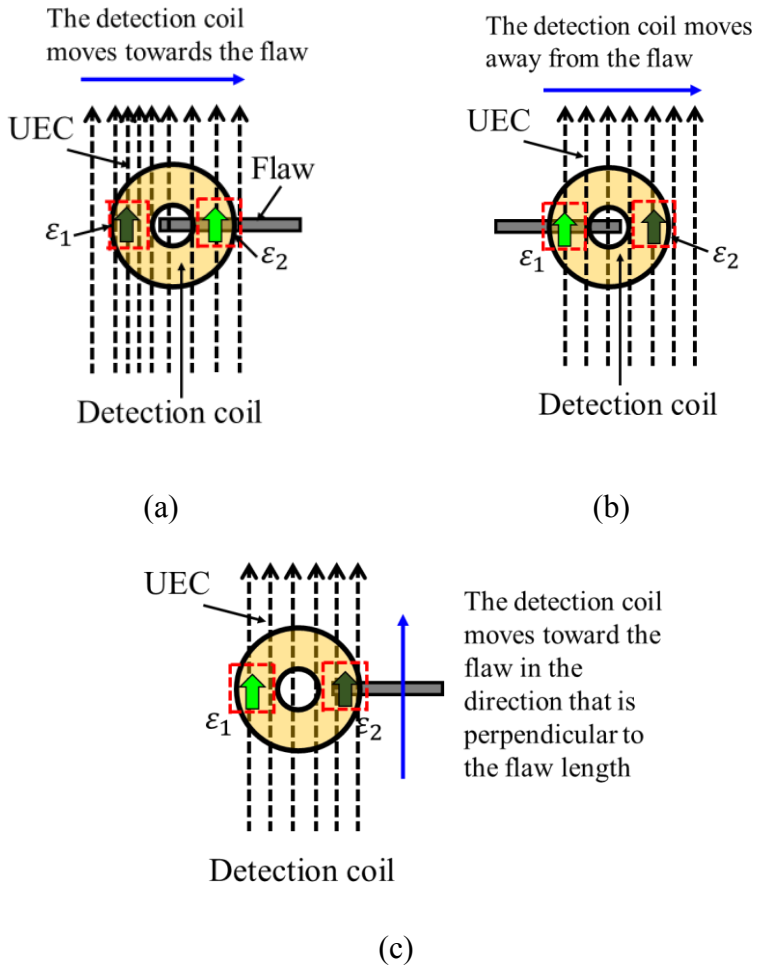

Figure 4.10 UEC distributions due to the movement of the BPRUEC (a) probe moving towards the flaw, (b) probe moving away from the flaw, and (c) probe moving toward the flaw perpendicular to the flaw length.

As described above, the amplitude of the two peaks of the detection signal on the edge of each flaw were not relatively the same. Moreover, in the measurement results of scanning #3, one peak of the detection signal on the edge of each flaw disappeared

because pair #1 of the excitation coils, whose induction was weak, was dominant in generating the signal when the BPRUEC was moving away to the edge of flaw parallel to the flaw length.

Finally, an essential requirement for improving the BPRUEC is to determine the ratio of the number of turns between the pair of excitation coils, the excitation currents for each pair of the excitation coils, and the structure between the excitation coils to generate the rotating UEC with the same amplitude in all directions. Determining the position to meet the right balance between the excitation and detection coils to ensure self-nulling characteristic for a high S/N ratio is another aspect that merits further investigation.

4.6. Summary

The Butterfly probes with rotating eddy current proposed have been used in experiments to detect varying flaws on aluminum plates. The conclusions of this study are as follows,

1. Implementation of the designed butterfly probes with rotating uniform eddy current to detect flaws on the aluminum plate presented.
2. Analysis by finite element simulation, the butterfly probe with two pairs of excitation coil succeeded in showing a uniform eddy current pattern rotates that having relatively almost the same amplitude in all directions.
3. The probe successfully detected flaws in all directions although the detectability of the probe, which its result was depend on scanning direction.
4. In the direction of scanning # 1 and # 2, butterfly probes with uniform eddy currents that rotate could clearly detect flaws; flaw length corresponds to the distance between

the two signal peaks produced. Meanwhile, relatively, the amplitude of the signal peaks relates to the flaw depth.

5. In the direction of scanning # 3 and # 4, the probe could detect flaws; the distance between the two peaks produced corresponds to the flaw length. However, the peak signal amplitude is lower than scanning # 1 and # 2 and tends to be not the same.
6. Detection signals from scanning # 1 and # 2, maximum energizing was dominated by pair #2 of excitation coil. Meanwhile, the detection signal from scanning # 3 and # 4, maximum energizing was dominated by pair # 1 of the excitation coil. In this case, the number of coil windings in pair # 2 is twice then pair # 1. This ratio causes the detection signal from scanning # 1 and # 2 to be higher.
7. The probe successfully showed the characteristics of self-differential and self-nulling with the signal amplitude that tends to zero when the probe is in the middle of a flaw.
8. The precise setting of the detection coil position in the middle of the crossing of two pairs of excitation coil is a determinant of the quality of the resulting measurement signal.

Chapter 5
5. Conclusion

5.1. Conclusion

Reviewing all the studies that have been described in all chapters, the following are the conclusions of this study;

1. A pair of pancake-oriented rectangular excitation coils from the butterfly probe have shown successful performance to increase the intensity of the uniform eddy current on the test piece. The detection signal becomes higher because of it.
2. The pancake-oriented circle detector coil, which set in the middle of the axis of the excitation coil pair, makes the probe have self-differential and self-nulling characteristics. This characteristic had shown from the testing where the detection signals would increase when the coil in unbalanced condition due to flaw and relatively zero under a balanced condition.
3. In its measurement, an artificial lines flaw represented by a detection signal that has two peaks. The distance of the two signal peaks represents the length of the flaw, and the amplitude of the peak signal represents the depth of the flaw.
4. The right sensitivity of the measurement signal is affected by the specifications of the excitation coils must be precisely the same, and the detection coil setting must be right in the middle of the axis of the excitation coils pair.

5. A rotating eddy current had success generated from two layers of excitation coils pair which arranged perpendicular each other. The uniform density of the rotating eddy current influenced by the precise arrangement of the position of the coils, and the ratio of number winding between the coils layer.

5.2. Recommendation for Further Work

Future studies are expected;

1. The application of butterfly probes to other test materials is needed to improve the design and to get a general model that can be used to measure other types of materials.
2. The coils structure of the BPRUEC must be calculated the precise ratio between the winding coil of pairs #1 and #2 for perfecting. In this work, the ratio was only set at 1:2 for simplicity.
3. To obtain a relatively uniform rotating eddy current density, the lift-off effect of the second layer of excitation coil on BPRUEC needs to be reduced by modification of the excitation coil structure using multi-layers. The multi-layer effect needs to be further observed.

References

1. J. Hansen. The eddy current inspection method, Insight Vol 46 No 5 May 2004.
2. L.S. Obrutsky, T. Harasym, V.S. Cecco and S.P. Sullivan, Transmit-Receive Eddy Current Probes for Defect, 3rd International CANDU Maintenance Conference, Toronto, November 19 – 21, 1995.
3. Hoshikawa, H.; Koyama, K. A New ECT Probe with Rotating Direction Eddy Current. In Review of Progress in Quantitative Nondestructive Evaluation. Thompson, D.O., Chimenti, D.E., Eds; Springer, Boston, MA, USA, 1996; Volumn 15A, pp. 1091–1098.
4. Rifai, D.; Abdalla, A. N.; Razali, R.; Ali, K.; Faraj, M. A. An eddy current testing platform system for pipe defect inspection based on an optimized eddy current technique probe design. *Sensors (Switzerland)* **2017**, *17*, doi:10.3390/s17030579.
5. Li, W.; Yuan, X.; Chen, G.; Ge, J.; Yin, X.; Li, K. High sensitivity rotating alternating current field measurement for arbitrary-angle underwater cracks. *NDT E Int.* **2016**, *79*, 123–131, doi:10.1016/j.ndteint.2016.01.003.
6. Blakeley, B.; Lugg, M. Application of ACFM for inspection through metal coatings. *Insight Non-Destructive Test. Cond. Monit.* **2010**, *52*, 310–315, doi:10.1784/insi.2010.52.6.310.
7. Papaelias, M. P.; Lugg, M. C.; Roberts, C.; Davis, C. L. High-speed inspection of rails using ACFM techniques. *NDT E Int.* **2009**, *42*, 328–335, doi:10.1016/j.ndteint.2008.12.008.
8. Dolapchiev, I. A New Eddy Current Surface Probe with Perpendicular Coils. *Mater. Sci. Forum* **2016**, *856*, 207–212, doi:10.4028/www.scientific.net/MSF.856.207.
9. Dogaru,T. and Smith, S. T. Giant Magnetoresistance-Based Eddy-Current Sensor. *IEEE Trans. Magn.* **2001**, *37*, 3831–3838.
10. Hoshikawa, H.; Koyama, K.; Karasawa, K. A new ECT surface probe without lift-off noise and with phase information on flaw depth. *AIP Conf. Proc.* **2001**, *20*, 969–976, doi:10.1063/1.1373861.
11. Lugg, M. C. The First 20 years of the A.C. field Measurement Technique. *18th World Conf. Nondestruct. Test.* **2012**, 7.

12. Sopian, A.; Y., T. G.; Rudlin, J.; Tailor, D. Electromagnetic and eddy current NDT: A review. *Insight Non-Destructive Test. Cond. Monit.* **2001**, *43*, 302–306, doi:10.1784/insi.2015.57.6.337.
13. Hoshikawa, H.; Koyama, K.; Naruse, Y. Detecting weld zone over anticorrosion painting by rotating uniform eddy current probe. *AIP Conf. Proc.* **2005**, *760*, 502–508, doi:10.1063/1.1916717.
14. Raine, A.; Lugg, M. A review of the alternating current field measurement inspection technique. *Sens. Rev. Vol. 19. Number 3. 1999. pp. 207±213* **1999**, *19. Number*, 207–213.
15. JNSDI, Eddy Current testing I, Japan Association Nondestructive Inspection, 1995.
16. JNSDI, Eddy Current testing III, Japan Association Nondestructive Inspection, 2003.
17. Garcí, J.; Gomez-Gil, J.E.V.-S. Non-Destructive Techniques Based on Eddy Current Testing. *Sensors* **2011**, *11*, 2525–2565.
18. Wei, L.; Guoming, C.; Xiaokang, Y.; Chuanrong, Z.; Tao, L. Analysis of the lift-off effect of a U-shaped ACFM system. *NDT E Int.* **2013**, *53*, 31–35, doi:10.1016/j.ndteint.2012.10.001.
19. Koyama, K.; Hoshikawa, H.; Mito, Y. Surface Flaw Testing of Weld Zone by Uniform Eddy Current Probe. *J. Japanese Soc. Non-Destructive Insp.* **2006**, *60*, 275–282, doi:https://doi.org/10.11396/jjsndi.60.275.
20. Hoshikawa, H.; Koyama, K. Uniform Eddy Current Probe with Little Disrupting Noise. *Rev. Prog. Quant. Nondestruct. Eval. Ed. by D.O. Thompson D.E. Chimenti, Plenum Press. New York,* **1998**, *17 A*, 1059–1066.
21. Le Bihana, Y., Lift-off and tilt effect on eddy current measurement: a 3-D finite element study. *Eur. Phys. JOURNAL, Appl. Phys.* **2002**, 25–28, doi:DOI: 10.1051/epjap:2001002.
22. Gao, P.; Wang, C.; Li, Y.; Cong, Z. Electromagnetic and eddy current NDT in weld inspection: A review. *Insight Non-Destructive Test. Cond. Monit.* **2015**, *57*, 337–345, doi:10.1784/insi.2015.57.6.337.
23. Hoshikawa, H.; Koyama, K. Uniform Eddy Current Probe with Little Disrupting Noise. In *Review of Progress in Quantitative Nondestructive Evaluation*; Thompson, D.O., Chimenti, D.E., Eds.; Plenum Press: New York, NY, USA, 1998; Volume 17A, pp. 1059–1066.
24. Teresa Restivo, M. A case study of induced eddy currents. *Sensors Actuators A. Phys.* 1995, *51*, 203–210.

25. Wincheski, B.; Fulton, J. P.; Nath, S.; Namkung, M.; Simpson, J. W. Self-nulling eddy current probe for surface and subsurface flaw detection. *Mater. Eval.* **1994**, *52*, 22–26, doi:10.1016/S0963-8695(97)82593-5.
26. Koyama, K.; Hoshikawa, H.; Kojima, G. Eddy Current Nondestructive Testing for Carbon Fiber- Reinforced Composites. *J. Press. Vessel Technol.* **2013**, *135*, 041501, doi:10.1021/cr050362v.
27. Auld, B. A.; Moulder, J. C. Review of Advances in Quantitative Eddy Current Nondestructive Evaluation. *J. Nondestruct. Eval.* **1999**, *18*, 3–36.
28. Hoshikawa, H.; Koyama, K.; Maeda, M. A New Eddy Current Surface Probe for Short Flaws with Minimal Lift-off Noise. Available Online: https://www.google.com/url?sa=t&source=web&rct=j&url=http://extras.springer.com/2003/978-0-7354-0117-4/cdr_pdfs/indexed/413_1.pdf&ved=2ahUKEwj9lfnL4_XfAhUMw7wKHVFDCmcQFjABegQIAxAB&usg=AOvVaw0UTmgf1AbGg6j17cqcTj-G (accessed on 18 January 2019).

29. Postolache, O.; Ramos, H. G.; Lopes Ribeiro, A.; Corrêa Alegria, F. GMR based eddy current sensing probe for weld zone testing. *Proc. IEEE Sensors* **2009**, 73–78, doi:10.1109/ICSENS.2009.5398524.
30. Vacher, F.; Alves, F.; Gilles-Pascaud, C. Eddy current nondestructive testing with giant magneto-impedance sensor. *NDT E Int.* **2007**, *40*, 439–442, doi:10.1016/j.ndteint.2007.02.002.
31. Cadugan, B. B. Application Information Allegro ICs Based on Giant Magnetoresistance (GMR). *Allegro MicroSystems* **2018**, 1–5.
32. Rifai, D.; Abdalla, A. N.; Ali, K.; Razali, R. Giant magnetoresistance sensors: A review on structures and non-destructive eddy current testing applications. *Sensors (Switzerland)* **2016**, *16*, doi:10.3390/s16030298.
33. Ditchburn, R. J.; Burke, S. K.; Posada, M. Eddy-current nondestructive inspection with thin spiral coils: Long cracks in steel. *J. Nondestruct. Eval.* **2003**, *22*, 63–77, doi:10.1023/A:1026340510696.
34. Abdilla, L.; Mangion, L.; Sammut, C. V. Eddy current sensing using planar coils. *IEEE Instrum. Meas. Mag.* **2012**, *15*, 14–18, doi:10.1109/MIM.2012.6365537.

35. Vilaca, P.; Santos, T. G.; Rosado, L.; Miranda, R. M. Innovative concept and application of EC probe for inspection of friction stir welds. *Int. J. Microstruct. Mater. Prop.* **2014**, *9*, 314–326, doi:10.1504/IJMMP.2014.066912.
36. Rosado, L. S.; Santos, T. G.; Piedade, M.; Ramos, P. M.; Vilaça, P. Advanced technique for non-destructive testing of friction stir welding of metals. *Meas. J. Int. Meas. Confed.* **2010**, *43*, 1021–1030, doi:10.1016/j.measurement.2010.02.006.
37. Yamada, S.; Katou, M.; Iwahara, M.; Dawson, F. P. Eddy current testing probe composed of planar coils. *IEEE Trans. Magn.* **1995**, *31*, 3185–3187, doi:10.1109/20.490322.
38. Papagiannopoulos, I.; De Mey, G.; Chatziathanasiou, V. Current distribution in circular planar coil. *Eng. Anal. Bound. Elem.* **2013**, *37*, 747–756, doi:10.1016/j.enganabound.2013.02.005.
39. Xie, R.; Chen, D.; Pan, M.; Tian, W.; Wu, X.; Zao, W.; Tang, Y.; Fatigue Crack Length Sizing Using a Novel Flexible Eddy Current Sensor Array. *Sensors* **2015**, *15*, 32138–32151, doi:10.3390/s151229911.
40. Rosado, L. S.; Santos, T. G.; Ramos, P. M.; Vilaça, P.; Piedade, M. A differential planar eddy currents probe: Fundamentals, modeling and experimental evaluation. *NDT E Int.* **2012**, *51*, 85–93, doi:10.1016/j.ndteint.2012.06.010.
41. Hosikawa, H.; Koyama, K.; Maeda, M.; Signal Phase Indication of Flaw Depth by A Lift-off Noise free Eddy Current Probe. *Rev. Quant. Nondestruct. Eval.* **2002**, *21*, 430–437.
42. Sekino, K.; Shimizu, K.; Fujimoto, T. Study on the Fundamental Characteristics of the Θ Probe and Crack Monitoring Using This Probe Combined with the Caustic Method. *J. Solid Mech. Mater. Eng.* **2008**, *2*, 115–127, doi:10.1299/jmmp.2.115.
43. Koyama, K.; Hoshikawa, H.; Basic Study of a New ECT Probe Using Uniform Rotating Direction Eddy Current. *Rev. Prog. Quant. Nondestruct. Eval.* **1997**, *16*, 1067–1074.
44. Theodoulidis, T. P.; Kriezis, E. E. Impedance evaluation of rectangular coils for eddy current testing of planar media. *NDT E Int.* **2002**, *35*, 407–414, doi:10.1016/S0963-8695(02)00008-7.
45. Santos, T. G.; Vilaça, P.; Quintino, L.; Dos Santos, J.; Miranda, R. M. Application of Eddy Current techniques to inspect friction spot welds in aluminium alloy AA2024 and a composite material. *Weld. World* **2011**, *55*, 12–18, doi:10.1007/BF03321315.

46. Rosado, L. S.; Santos, T. G.; Ramos, P. M.; Vilaça, P.; Piedade, M. A new dual driver planar eddy current probe with dynamically controlled induction pattern. *NDT E Int.* **2015**, *70*, 29–37, doi:10.1016/j.ndteint.2014.09.009.
47. B.P.C. Rao Eddy current testing: Basics. *J. Non Destr. Test. Eval.* **2011**, *10*, 1–16.
48. Kriezis, E. E.; Tsiboukis, T. D.; Panas, S. M.; Tegopoulos, J. a. Eddy currents: theory and applications. *Proc. IEEE* **1992**, *80*, 1559–1589, doi:10.1109/5.168666.
49. Sheng, X.; Li, Y.; Lian, M.; Xu, C.; Wang, Y. Influence of Coupling Interference on Arrayed Eddy Current Displacement Measurement. *Mater. Eval.* **2016**, *74*, 1675–1683.
50. Repelianto, A.S.; Kasai, N. The improvement of flaw detection by the configuration of uniform eddy current probes. *Sensors* **2019**, *19*, 397, doi:10.3390/s19020397.
51. Yusa, N.; Janousek, L.; Rebican, M.; Chen, Z.; Miya, K.; Chigusa, N.; Ito, H. Detection of embedded fatigue cracks in Inconel weld overlay and the evaluation of the minimum thickness of the weld overlay using eddy current testing. *Nucl. Eng. Des.* **2006**, *236*, 1852–1859.
52. Postolache, O.; Artur Lopes Ribeiro, A.L.; Ramos, H.G.; GMR array uniform eddy current probe for defect detection in conductive specimens, Measurement 46 (2013) 4369–4378, http://dx.doi.org/10.1016/j.measurement.2013.06.050
53. Repelianto, A.S.; Kasai, N.; Sekino, K.; Masaki, M. A Uniform eddy current probe with a double-excitation coil for flaw detection on aluminium plates. *Metals* **2019**, 9, 1116; doi:10.3390/met9101116
54. Tumanski, S. Modern magnetic field sensors-a review. *Organ* **2013**, *10*, 1–12.
55. Sukhorukov, V.V.; Slesarev, D.A.; Vorontsov, A.N. Electromagnetic Inspection and Diagnostics of Steel Ropes: Technology, Effectiveness and Problems. *Mater. Eval.* **2014**, *72*, 1019–1027.
56. Hamia, R.; Cordier, C.; Dolabdjian, C. Eddy-current non-destructive testing system for the determination of crack orientation. *NDT E Int.* **2014**, *61*, 24–28, doi:10.1016/j.ndteint.2013.09.005.
57. Rocha, T.J.; Ramos, H.G.; Lopes Ribeiro, A.; Pasadas, D.J. Magnetic sensors assessment in velocity induced eddy current testing. *Sens. Actuators A Phys.* **2015**, *228*, 55–61, doi:10.1016/j.sna.2015.02.004.
58. Hur, D.H.; Choi, M.S.; Shim, H.S.; Lee, D.H.; Yoo, O. Influence of signal-to-noise ratio on eddy current signals of cracks in steam generator tubes. *Nucl. Eng. Technol.* **2014**, *46*, 883–888.

59. Repelianto, A.S.; Kasai, N. The improvement of flaw detection by the configuration of uniform eddy current probes. *Sensors* **2019**, *19*, 397.
60. AbdAlla, A.N.; Faraj, M.A.; Samsuri, F.; Rifai, D.; Ali, K.; Al-Douri, Y. Challenges in improving the performance of eddy current testing: Review. *Meas. Control (UK)* **2019**, *52*, 46–64, doi:10.1177/0020294018801382.
61. Anil, K.S.; Umar, S.; Sasi, B.; Thirunavukkarasu, S.; Rao, B.P.C. Development of Eddy Current Probe for Detection of Deep Sub-Surface Defects. *IETE Tech. Rev.* **2016**, *33*, 386–395. doi:10.1080/02564602.2015.1113145.
62. Raude, A.; Sirois, M.; Lemieux, H.; Crepeau, J. Advances in Carbon Steel Weld Inspection using Tangential Eddy Current Array. In Proceedings of the 19th World Conference on Non-Destructive Testing 2016, Munich, Germany, 13–17 June 2016. Available online: https://www.ndt.net/article/wcndt2016/papers/we2c5.pdf
63. Dogaru, T. Deep Crack Detection around Fastener Holes in Airplane Multi-Layered Structures Using GMR-Based Eddy Current Probes. *AIP Conf. Proc.* **2004**, *700*, 398–405, doi:10.1063/1.1711650.
64. Ye, C.; Anders, R.; Mahmoodul, H.; Erik, S.; Lalita, U.; Satish, U. EC probe with orthogonal excitation coils and TMR sensor for CFRP inspection. *Int. J. Appl. Electromagn. Mech.* **2019**, *59*, 1247–1255, doi:10.3233/JAE-171193.
65. Laenen, C.; Salazar, G.; Topp, D. Application of the ACFM inspection method for the inspection of internal tank welds. *IV Conf. Panam. END* **2007**, 13, doi:10.1109/PESC.2004.1355225.

List of Publication

A. International Journal

1. The Improvement of Flaw Detection by the Configuration of Uniform Eddy Current Probes; Review, A. S. Repelianto, N. Kasai on *Sensors* 2019, 19, 397
2. A Uniform Eddy Current Probe with a Double-Excitation Coil for Flaw Detection on Aluminium Plates, A. S. Repelianto, N. Kasai, K. Sekino, M. Masaki on Metals; Special issue on Metals 2019, 9, 1116; doi:10.3390/met9101116
3. Flaw detection in aluminum plates using a rotating uniform eddy current probe with two pairs of excitation coils, A. S. Repelianto, N. Kasai, K. Sekino, M. Masaki, L. Q. Trung on Metals; Special issue, *Metals* 2019, *9*, 1069; doi:10.3390/met9101069

B. International Conference

A. S. Repelianto, N. Kasai, K. Sekino, M. Masaki. "Development of Uniform eddy current probe using double excitation coils on the aluminum plate", Presentation on Asia Pacific Symposium on Safety 2019, September 19-21, 2019, Dalian China.

C. Domestic Conference

1. A. S. Repelianto, N. Kasai, K. Sekino. "Investigation of the flaw detectability of Uniform Eddy Current Probes", Japan Society of Mechanical Engineers 2019 annual conference, September 9-11, 2019, Akita university, Japan.
2. A. S. Repelianto, N. Kasai, K. Sekino, M. Masaki. "New uniform eddy current probe for flaws detection on the aluminum plates", Japan Society of Mechanical Engineers 2019 annual conference, September 9-11, 2019, Akita university, Japan.
3. A. S. Repelianto, N. Kasai, K. Sekino. "Development of Uniform eddy current probe for improvement of defect detection on the metal material", Industrial, Chemical Machinery and Safety Division Conference 2018 Autumn, November 16, 2018, Shinjuku, Japan.
4. Le Quang Trung, Naoya Kasai, Ageng S. Repelianto, Kouichi Sekino, Matsunaga Masaki, "Study on A New Uniform Eddy Current Probe for Cracks Detection", Japan Society for Safety Engineering 2019, November 28, 2019, Nigata, Japan.
5. M. Matsunaga, N. Kasai, Ageng S. Repelianto, Le Q. Trung, K. Sekino, Simulation Analysis of Eddy Current Probe with Multi-coils, conference: Industrial and chemical-mechanical and safety department study, JSME, Dec 20, 2019, Polytechnic University, Kodaira City, Tokyo.

6. Ageng S. Repelianto, Naoya Kasai, Kouichi Sekino, Matsunaga Masaki, Le Quang Trung, A new rotating uniform eddy current probe for detecting flaws in aluminum plates, The 23rd symposium of JSNDI, Electromagnetic Application Division, Magnetic Powder, Penetration, Visual Division, Leak Test Division on Sound diagnosis and quality inspection using surface flaw detection technology, March 17-18, 2020, Tokyo.